Hindawi Publishing Corporation
Advances in Condensed Matter Physics
Volume 2015, Article ID 391579, 20 pages
http://dx.doi.org/10.1155/2015/391579

Review Article

Indentation Depth Dependent Mechanical Behavior in Polymers

Farid Alisafaei and Chung-Souk Han

Department of Mechanical Engineering, University of Wyoming, 1000 E. University Avenue, Laramie, WY 82071, USA

Correspondence should be addressed to Chung-Souk Han; chan1@uwyo.edu

Received 20 April 2015; Accepted 9 July 2015

Academic Editor: Victor V. Moshchalkov

Various experimental studies have revealed size dependent deformation of materials at micro and submicron length scales. Among different experimental methods, nanoindentation testing is arguably the most commonly applied method of studying size effect in various materials where increases in the hardness with decreasing indentation depth are usually related to indentation size effects. Such indentation size effects have been observed in both metals and polymers. While the indentation size effects in metals are widely discussed in the literature and are commonly attributed to geometrically necessary dislocations, for polymer the experimental results are far sparser and there does not seem to be a common ground for their rationales. The indentation size effects of polymers are addressed in this paper, where their depth dependent deformation is reviewed along with the rationale provided in the literature.

1. Introduction

Nanoindentation is one of the most commonly applied methods for determining of material properties and characterization of deformation behavior at nano- to micrometer length scales. Performing nanoindentation experiments, the mechanical behavior of various materials has been found to be dependent on the indentation depth indicating changing deformation mechanisms with the length scale. Length scale dependent deformation has been experimentally observed in different materials including metals and polymers. In metals, size dependent deformation has been reported in micro- and nanoindentation tests of bulk materials [1–7], microsized beam bending experiments [8], microtorsion of thin wires [9], tension of perforated plates [10, 11], nanoindentation of thin films [12], particle-reinforced metal matrix composites [13, 14], and so forth. Similar to metals, length scale dependent deformation has been also experimentally observed in polymers at micro to submicron length scales by nanoindentation [15, 16], microsized beam bending experiment [17, 18], and bending test of nanofibers [19, 20], as well as in particulate reinforced composites (a relatively recent review can be found in [21]). The length scale dependent deformation has been experimentally observed in various polymers such as epoxy [16, 17, 22–27], polycarbonate (PC) [15, 16, 28], polystyrene (PS) [15, 28], polymethyl methacrylate (PMMA) [15, 28, 29], polydimethylsiloxane (PDMS) [30–35], silicon rubber/elastomer [36–38], nylon (PA66) [39], polypropylene (PP) [18], polyimide (PI) [40], polyvinyl chloride (PVC) [28], polyamide 6 (PA6) [41], and polystyrene acrylonitrile (SAN) [28].

In metals, length scale dependent deformation is usually associated with geometrically necessary dislocations [42, 43] resulting in an increase of strain gradients with decreasing length scale [44–48]. In polymers, however, such a notion is not applicable and different explanations have been suggested in the literature as a rationale for such size effects including higher order displacement gradient models [16, 17, 22–25, 29, 33, 49–51], surface effects [36, 52], changes in the material properties through thickness (heterogeneity of the material) [15, 31], and friction [34]. Due to the complex and varied molecular structures of polymers, the mechanisms of the abovementioned length scale dependent deformations in polymers are arguably more complicated than in metals. Furthermore, as polymers are known to be rate and temperature sensitive, such length scale dependent deformations in polymers should be more affected by rate/temperature changes than in metals.

While length scale dependent deformation in polymers has been observed in different experiments including bending of microbeams, nanoindentation, bending of nanofiber and particulate-reinforced composites, in this paper, the

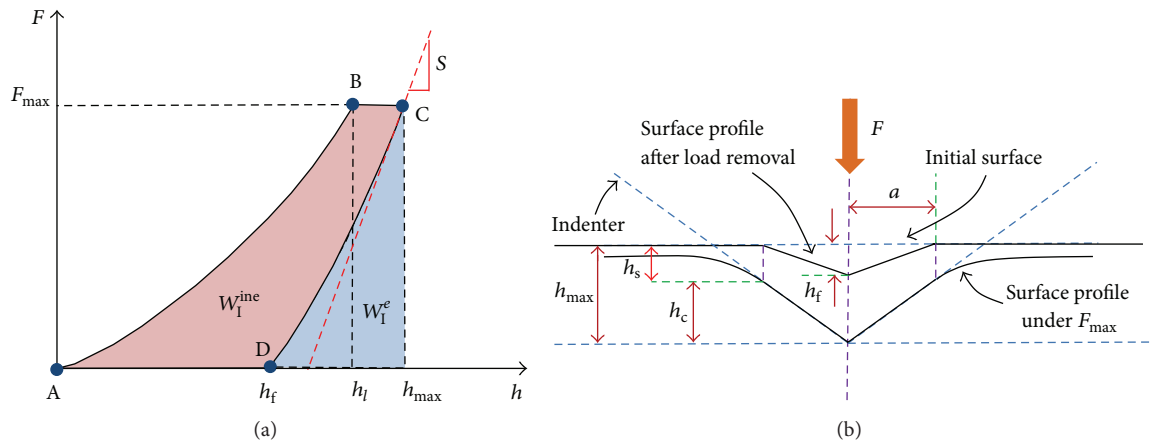

FIGURE 1: (a) Schematic representation of load-displacement curve in nanoindentation testing. (b) Schematic representation of cross section through indentation of a material sample.

TABLE 1: Projected contact area, surface area, angles, geometric constants, and geometry correction factors for common indenter geometries [55] where h_c is the contact depth (shown in Figure 1(b)), h is the indentation depth under applied force F (see Figure 1(a)), R is the radius of spherical tip, θ is the semiangle of indenter tip (for pyramidal tips θ is the face angle with the central axis of the tip [55]), α is the half angle defining an equivalent cone, ϵ is the geometric constant (for the pyramidal tips ϵ is theoretically 0.72; however, a value of 0.75 has been experimentally found to better represent experimental data [55]), and β is the geometry correction factor used for the determination of elastic modulus [53]. Note that A_c and A_s given in Table 1 for Berkovich, Vicker, Knoop, cube corner, and cone indenters are, respectively, the projected and surface areas of a perfectly sharp indenter without imperfection/bluntness (see, e.g., [53, 55], for the projected contact area of a blunt indenter).

Indenter tip	Projected contact area A_c	Surface area A_s	Semiangle θ (deg)	Effective cone angle α (deg)	Geometric constant ϵ	Geometry correction factor β
Sphere	$\pi(2h_cR - h_c^2)$	N/A	N/A	N/A	0.75	1
Berkovich (perfect)	$3\sqrt{3}h_c^2 \tan^2\theta$	$3\sqrt{3}h^2 \tan\theta/\cos\theta$	65.03°	70.3°	0.75	1.034
Berkovich (modified)	$3\sqrt{3}h_c^2 \tan^2\theta$	N/A	65.27°	70.3°	0.75	1.034
Vicker	$4h_c^2 \tan^2\theta$	$4h^2 \sin\theta/\cos^2\theta$	68°	70.3°	0.75	1.012
Knoop	$2h_c^2 \tan\theta_1 \tan\theta_2$	N/A	$\theta_1 = 86.25°$ $\theta_2 = 65°$	77.64°	0.75	1.012
Cube corner	$3\sqrt{3}h_c^2 \tan^2\theta$	N/A	35.26°	42.28°	0.75	1.034
Cone	$\pi h_c^2 \tan^2\alpha$	N/A	α	α	0.727	1

length scale dependent deformation in polymers observed with indentation experiments is reviewed along with the notions on its physical origin as well as theoretical models that predict such length scale dependent deformations in polymers. In Section 2, the length scale dependent deformation of polymers observed in nanoindentation testing is critically reviewed followed by discussions on the possible explanations for the origin of length scale dependent deformation in polymers in Section 3.

2. Size Dependent Deformation of Polymers Observed in Nanoindentation Experiments

To set the stage and clarify the notation, Figure 1(a) shows a schematic load-displacement curve of nanoindentation consisting of loading (section A-B), holding (section B-C), and unloading (section C-D) sequences [25]. A corresponding schematic cross section of such an indentation is depicted in Figure 1(b) identifying parameters used in the analysis [53, 54] which will be discussed later.

2.1. Hardness and Elastic Modulus Determination. Similar to metals [2], the hardness parameter (indentation hardness [53] and universal hardness [54]) is usually used to investigate the indentation size effect (ISE) in polymers [15, 22]. Indentation hardness H_I can be obtained as

$$H_I = \frac{F_{max}}{A_c}, \tag{1}$$

where F_{max} is the maximum applied force (shown in Figure 1(a)) and A_c is the projected contact area at the maximum applied force F_{max}. The projected contact area A_c as a function of contact depth h_c (see Figure 1(b)) for some common indenter geometries is given in Table 1 [55]. As can be seen in Figure 1(b), the contact depth h_c is determined by

$$h_c = h_{max} - h_s, \tag{2}$$

where h_{max} is the indentation depth h at the maximum applied force F_{max} before the unloading section (see Figure 1) and h_s is determined by

$$h_s = \epsilon \frac{F_{max}}{S} \tag{3}$$

in which S is the initial slope of unloading curve (see Figure 1(a)) and ϵ is a geometric constant given in Table 1 for different tip geometries. To determine the stiffness S by the Oliver and Pharr approach [53], the unloading curve of Figure 1(a) is described as

$$F = B\left(h - h_f\right)^m, \tag{4}$$

where the parameters B, m, and h_f are obtained by fitting the upper portion of unloading curve. Thus, S is determined by taking the derivative of F with respect to h in (4) at the maximum applied force F_{max} shown in Figure 1(a). In addition to the indentation hardness H_I, the universal hardness H_U (also known as Martens hardness) can be also determined from nanoindentation tests. The universal hardness for a perfect Berkovich (unmodified Berkovich) and Vicker tips is defined as follows:

$$H_U = \frac{F}{A_s}, \tag{5}$$

where A_s is the surface area under the initial surface (see Figure 1(b)) given in Table 1 as a function of indentation depth h. As mentioned above, the indentation size effect of materials is usually described by measuring the hardness (H_I and/or H_U) at different indentation depths ranging from microns to few nanometers. However, in contrast to metals [56, 57], in polymers length scale dependent deformation has been also experimentally observed by monitoring the elastic modulus determined from indentation experiments by various approaches with sharp indenter tips which will be denoted as indentation elastic modulus in the following. The indentation elastic modulus of materials is often obtained following Oliver and Pharr (O&P) [53] as

$$E_r^{O\&P} = \frac{\sqrt{\pi} S}{2\beta\sqrt{A_c}}, \tag{6}$$

where β is the tip geometry correction factor (see Table 1) and $E_r^{O\&P}$ is the reduced elastic modulus [53] which is related to the elastic modulus of polymer, $E^{O\&P}$, via

$$\frac{1}{E_r^{O\&P}} = \frac{1-\nu^2}{E^{O\&P}} + \frac{1-\nu_i^2}{E_i} \tag{7}$$

in which E_i and ν_i are, respectively, the elastic modulus and Poisson's ratio of indenter tip with ν being the Poisson's ratio of the polymer.

2.2. Indentation Size Effect in Polymers. The indentation size effects of various polymers are depicted in Figure 2 where the indentation hardness H_I increases with decreasing h_{max} [15, 16, 26, 36, 39]. Therein, it can be seen that there is a significant rise in the indentation hardness of epoxy [16, 26], polycarbonate (PC) [15, 16], polystyrene (PS) [15], polymethyl methacrylate (PMMA) [15], silicon elastomer [36], and nylon (PA66) [39] as h_{max} decreases. However, H_I of ultra-high molecular weight polyethylene (UHMWPE) [15] remains almost constant for $h_{max} > 100$ nm where there is only a slight increase in the indentation hardness of UHMWPE at very shallow indentation depths $h_{max} < 100$ nm which will be discussed later. Similar to the trend observed for the indentation hardness of polymers in Figure 2, length scale dependent deformation of polymers can be also observed in Figure 3 where the universal hardness, H_U, increases with decreasing h_{max} [15, 25, 28]. Comparing H_I of Figure 2 with H_U of Figure 3, the indentation hardness is found to be slightly higher than the universal hardness as the projected contact area A_c (see (1)) is usually smaller than the surface area A_s used in (5) [25].

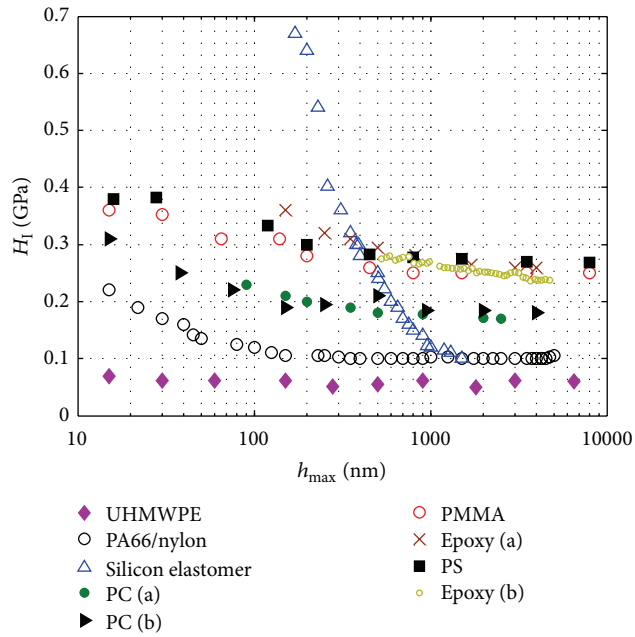

FIGURE 2: Indentation hardness H_I versus h_{max} for various polymers redrawn from [15] (UHMWPE, PC (b), PMMA, PS), [16] (PC (a), epoxy (a)), [26] (epoxy (b)), [36] (silicon elastomer), and [39] (PA66/nylon).

Generally, due to the complex structures of polymers and their rate, temperature, and pressure dependence behavior, in addition to the higher order displacement gradient effects, indentation size effects can be caused by various sources. These sources include but are not restricted to surface effect [36, 52], change in the glass transition temperature [41], adhesion [59, 60], tip bluntness [61], material inhomogeneity [15], and confined molecular motion interfacial region (formation of an interfacial region of confined molecular motion between the surface and probe by contact loading) [62].

It can be seen in Figures 2 and 3 that the characteristics of length scale dependent deformation in polymers significantly differ from polymer to polymer. As shown in Figures 2 and 3, the depth h_{max} at which the hardness starts to noticeably

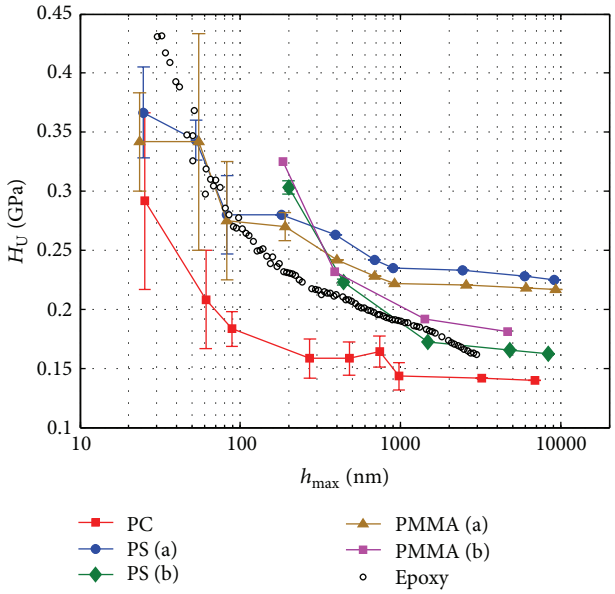

FIGURE 3: Universal hardness H_U versus h_{max} for various polymers redrawn from [15] (PC, PS (a), PMMA (a)), [28] (PS (b), PMMA (b)), and [25] (epoxy with 5 s loading time).

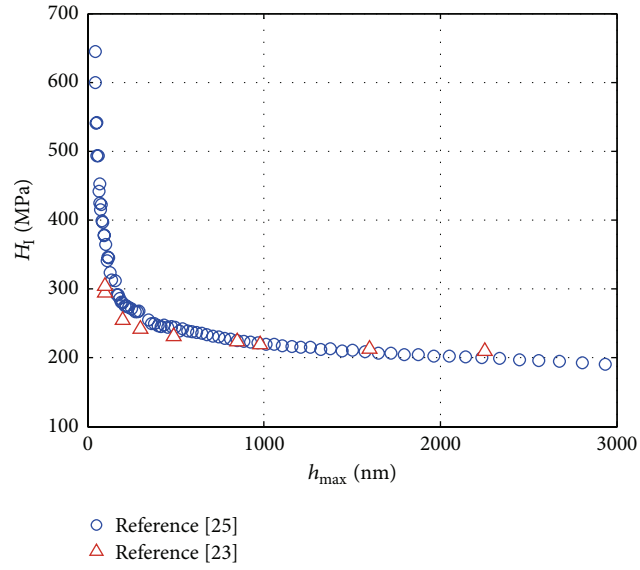

FIGURE 4: Indentation hardness of epoxy with 20 phr from [25] (with 20 s loading, holding, and unloading times) and [23] (with a constant loading and unloading rate of 1% of the maximum applied force with a 10 s holding time) obtained by the Oliver and Pharr approach [53].

increase can be remarkably different for different polymers [67]. For instance, the hardness of epoxy starts to increase below about $h_{max} = 3\,\mu$m [16, 25, 26], while for PC, PS, and PMMA hardness starts to rise below about $1\,\mu$m [15, 16]. Such an increase of hardness in PA66/nylon is only observed for $h_{max} < 200$ nm [39] where there is no increase in the hardness of UHMWPE for $h_{max} > 100$ nm [15] indicating that the characteristics of length scale dependent deformation can strongly vary in different polymers [68]. Furthermore, the increase in the hardness is significantly different in different polymers. In epoxy [16], PC [15, 16], PS [15], and PMMA [15] H_I increases by a factor of about 1.3 and in silicon elastomer [36] by a factor of about 6.7 for the indentation depth range of around 2 to $0.2\,\mu$m, while no size effect is observed in UHMWPE [15] and polytetrafluoroethylene (PTFE) [69] for the same indentation depth range of about 2 to $0.2\,\mu$m. In the following, the indentation size effect of polymers in the literature is reviewed in three polymer categories of thermosets, thermoplastics, and elastomers.

2.2.1. Thermoset Polymers. In addition to the microsized beam bending experiment [17], length scale dependent deformation of epoxy has been experimentally observed by nanoindentation testing in various studies [16, 22–27]. Length scale dependent deformation of thermoset epoxy was first observed in [16, 22] where the indentation hardness, H_I, of epoxy with 10 parts per hundred resin (phr) was found to increase with decreasing h_{max} as shown in Figure 2. Nanoindentation tests of [16] were performed by a sharp Berkovich tip in load-controlled mode with a constant loading and unloading rate of $0.01F_{max}$. The indentation hardness of epoxy (see (1)) was determined according to Oliver and Pharr [53] where a 10 s holding time (sections B-C in Figure 1(a)) was applied to minimize viscous effects. To ensure the accuracy of the hardness data H_I, the projected contact area A_c at each test was measured by atomic force microscopy (AFM) and compared with the one determined by the unloading curve (see (2)) where good agreement was achieved between the measured (AFM method) and determined (O&P method) contact areas.

Such length scale dependent deformation of epoxy was also experimentally observed in [26] with a Berkovich indenter tip at an indentation depth range between 4500 and 500 nm. Nanoindentation tests in [26] were performed in load-controlled mode with the following sequences: loading segment with a constant strain rate of $0.05\,s^{-1}$ until the maximum applied force F_{max} followed by a holding time of 10 s at the maximum applied force; unloading segment with a constant unloading rate equal to 70% of the loading rate until 80% of the maximum applied force F_{max} is removed; a second holding period of 2 s followed by a final unloading segment until F_{max} is completely removed. Indentation hardness of epoxy determined according to [53] as a function of h_{max} is plotted in Figure 2 where each point represents an average value of ten indents.

Performing nanoindentation tests with a sharp Berkovich indenter tip, the indentation size effect in epoxy has been also experimentally observed in [25] where H_I increases with decreasing h_{max} as shown in Figure 4. Taking the effects of tip bluntness/imperfection into account, it was shown that, for a sharp Berkovich tip with a tip roundness of about 40 nm, tip bluntness becomes significant only at $h_{max} < 250$ nm as illustrated in Figure 5 (see [25] for tip roundness determination). As the indentation size effect is observed at large depths far above $h_{max} \approx 250$ nm, it was concluded in

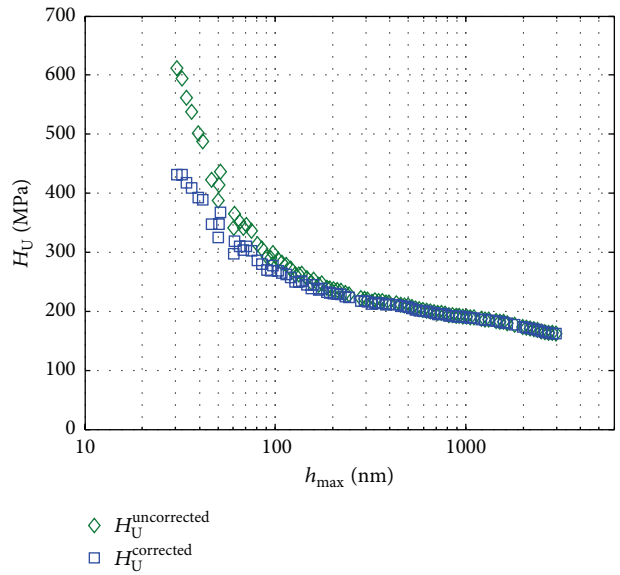

FIGURE 5: Effect of tip bluntness on the indentation size effect in epoxy with 20 phr ($H_U^{corrected}$ and $H_U^{uncorrected}$ represent the universal hardness with and without considering the effect of tip bluntness, resp.) [25].

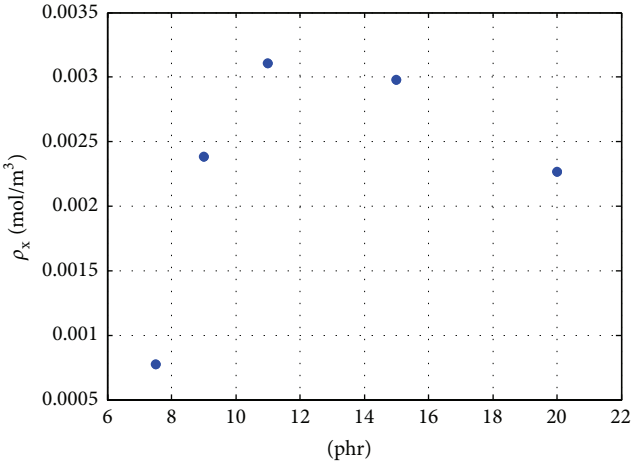

FIGURE 6: Cross-link density of epoxy as a function of hardener percentage [23].

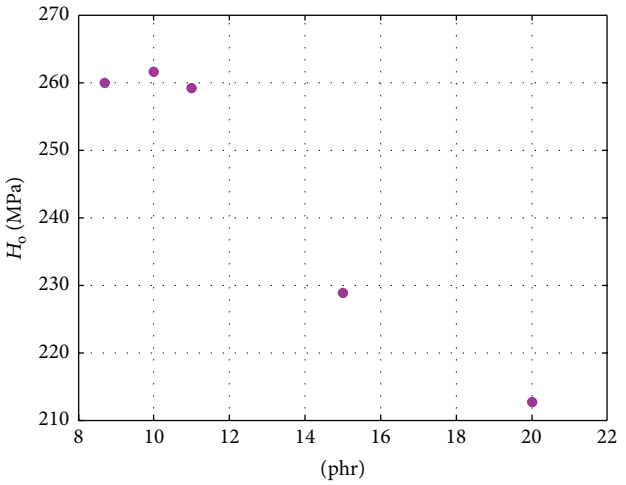

FIGURE 7: Indentation hardness of epoxy at large indentation depth h_{max} as a function of hardener percentage [23].

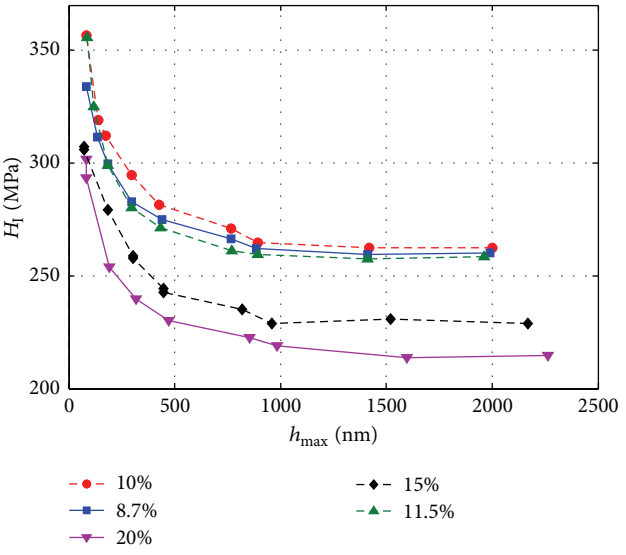

FIGURE 8: Indentation hardness of epoxy with different hardener contents as a function of indentation depth h_{max} [23].

[25] that the tip bluntness cannot explain such size effect in epoxy.

The effect of cross-link density on the length scale dependent deformation of epoxy was investigated in [23] by varying the hardener content. To this end, the cross-link density ρ_x of epoxy resin cured with varying amount of hardener content was first determined by dynamic mechanical tests. In Figure 6, the cross-link density of epoxy determined from the dynamic mechanical tests is plotted for the hardener contents (phr) of 7.5, 9, 11, 15, and 20. The highest cross-link density was observed at 11 phr where ρ_x decreases from its peak value on both sides [23]. Performing nanoindentation tests with the same experimental details of [16] mentioned above, the indentation hardness of epoxy with different hardener percentages was determined as a function of indentation depth. Figure 7 depicts the indentation hardness of epoxy at large indentation depths, H_o, for different hardener contents (phr) of 8.7, 10, 11, 15, and 20. The maximum value of H_o was observed at 11 phr where cross-link density ρ_x reaches its maximum value [23]. As H_o (indentation hardness at large depths where size effect is negligible) is directly proportional to the yield stress, Figure 7 implies that the yield stress of epoxy decreases with ρ_x. Using a sharp three-sided Berkovich tip, the indentation hardness H_I as a function of h_{max} is depicted in Figure 8 for the hardener contents (phr) of 8.7, 10, 11, 15, and 20. Length scale dependent deformation of epoxy is observed in Figure 8 where indentation hardness of epoxy increases with decreasing h_{max} for all phr hardener values. Analyzing the hardness data of Figure 8, it was observed that the length scale dependent deformation of epoxy becomes

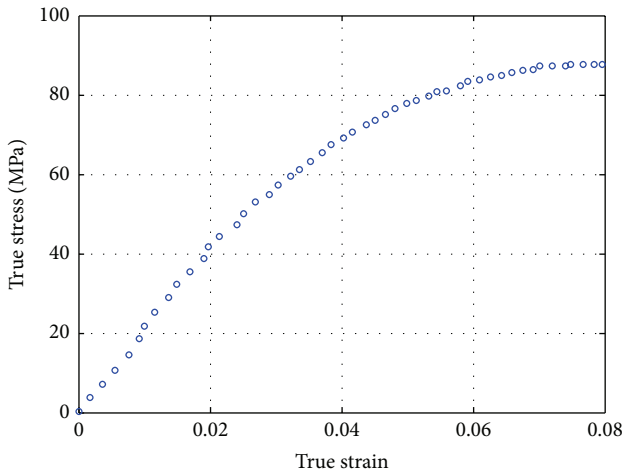

FIGURE 9: Compressive true stress-strain curve of 20 phr epoxy samples [24].

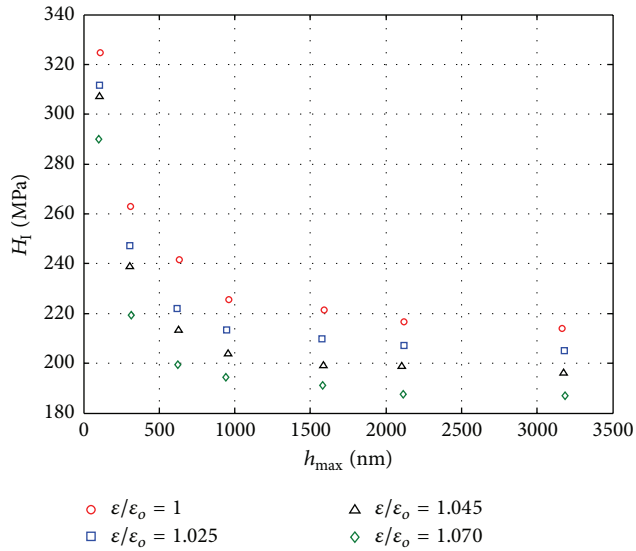

FIGURE 10: Indentation hardness of prestrained epoxy (20 phr) where ε and ε_o are, respectively, prestrain level and initial uniaxial yield strain [24].

more significant with increasing cross-link density. The effect of cross-link density on the size effect of epoxy observed in [23] is consistent with results presented in [34] which will be later discussed. It should be mentioned that epoxy samples of [23] were prepared in the same way as in [16] where both liquid resin (bisphenol A epichlorohydrin) and curing agent (diethylenetriamine) were mixed and cast into a rectangular Teflon crucible. As the curing agent of epoxy is hydrophilic while Teflon surface and open air are hydrophobic, such opposing tendencies may potentially cause depletion of curing agent from the surface of epoxy samples and segregation of resin and curing agent [23]. If curing agent is segregated from resin, then the surface region should contain less curing agent than the interior region of the sample. Subsequently, the hardness should be lower at small indentation depths close to the surface of the sample. However, an opposite trend is observed in Figure 8 where indentation hardness of epoxy increases with decreasing indentation depth h_{max} indicating that the length scale dependent deformation of epoxy is not associated with the segregation of curing agent during sample preparation [23].

The effect of plastic strain/deformation on the length scale dependent deformation of epoxy was studied by Lam and Chong [24]. Prismatic epoxy specimens with 20 phr were first loaded between two parallel glass platens (uniaxial compression) to induce plastic strain. Figure 9 shows the compressive stress-strain behavior of unprestrained epoxy where material hardening is observed with increasing compression. After compressive prestraining, nanoindentation testing was performed on the optically smooth side of epoxy samples orthogonal to the loading direction [24]. All nanoindentation tests were conducted in a displacement controlled mode with a Berkovich tip at an indentation range of 3.2 to 0.1 μm. A 10 s holding time was employed at the maximum applied load F_{max} to minimize time dependent effects. Results obtained from the nanoindentation tests are depicted in Figure 10 where indentation hardness H_I (obtained by the Oliver and Pharr approach [53]) is plotted as a function of indentation depth h_{max} for plastically prestrained epoxy samples. In contrast to Figure 9, the hardness of epoxy (depicted in Figure 10) decreases as prestraining increases. The decrease in the hardness of prestrained epoxy samples was attributed to the Bauschinger effect [24]. The Bauschinger effect has been experimentally observed in polymers when a prismatic specimen compressively prestrained in the uniaxial direction exhibits softening when it is compressed in the orthogonal direction [70]. Similarly, indentation hardness H_I in the orthogonal direction decreases with inducing prestrain as a result of Bauschinger effect [24]. Taking the Bauschinger effect into account, an energy based methodology was presented in [24] to separate the size effect from the prestrain softening effect (Bauschinger effect). As shown in Figure 11, after correcting for the Bauschinger effect, the indentation hardness H_I increases with increasing plastic strain which is in agreement with the hardening behavior observed in Figure 9. It is seen in Figure 11 that size effect in epoxy diminishes with increasing plastic deformation.

In addition to epoxy, indentation size effect of thermoset PMR-15 polyimide has been also studied in the literature. Redrawn from [40], the indentation hardness of PMR-15 polyimide as a function of indentation depth is depicted in Figure 12. A sharp Berkovich tip with a nominal tip radius of $r < 20$ nm was used to determine the indentation hardness of Figure 12 where a 2 s loading time was applied for all indentation tests. Creep effects were also taken into account in [40] for the determination of H_I of Figure 12 where h_{max} in (2) was replaced by $h_{max} - h_{creep}$ with h_{creep} being the change in the indentation depth during the holding time and S in (3) was replaced by S_e which is the elastic contact stiffness with considering the creep effect

$$\frac{1}{S_e} = \frac{1}{S} - \frac{\dot{h}_v}{\dot{P}}, \tag{8}$$

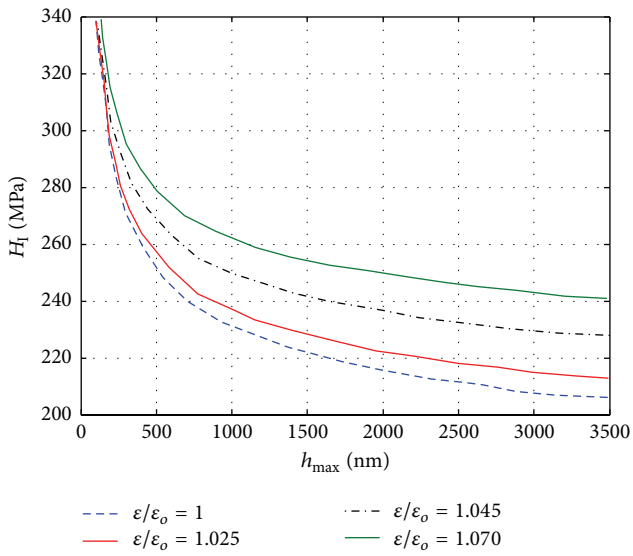

FIGURE 11: Indentation hardness of 20 phr epoxy after correction for the Bauschinger effect where ε and ε_o are, respectively, prestrain level and initial uniaxial yield strain [24].

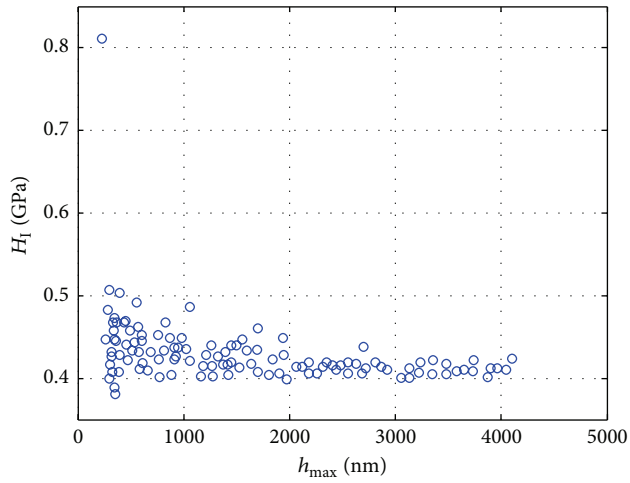

FIGURE 12: Indentation hardness of PMR-15 polyimide with a Berkovich tip [40].

where $\dot{h}_v$ is the creep rate at the end of the holding time and $\dot{P}$ is the unloading time. Thus, the contact depth h_c of (2) is determined as

$$h_c = \left(h_{max} - h_{creep}\right) - \epsilon F_{max}\left(\frac{1}{S} - \frac{\dot{h}_v}{\dot{P}}\right). \quad (9)$$

It is seen in Figure 12 that indentation size effect in PMR-15 polyimide is less pronounced than in epoxy and becomes noticeable only at shallow indentation depths of $h_{max} <$ 500 nm [40].

2.2.2. Thermoplastic Polymers. Performing nanoindentation tests with a Berkovich indenter tip, indentation size effect of four thermoplastic polymers PC, PS, PMMA, and UHMWPE was investigated by Briscoe et al. [15]. The effect of tip

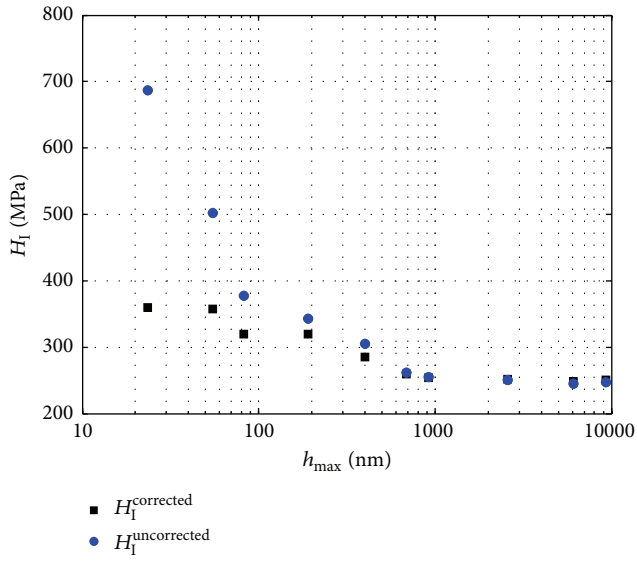

FIGURE 13: Effect of tip bluntness on the indentation size effect in PMMA ($H_I^{corrected}$ and $H_I^{uncorrected}$ represent the indentation hardness with and without considering the effect of tip bluntness, resp.) where 10 s loading, holding, and unloading times together with strain rate of 0.1 s^{-1} were imposed [15].

bluntness/imperfection on the size effect of PMMA is depicted in Figure 13 where $H_I^{corrected}$ (indentation hardness H_I obtained by a calibrated area function) starts to deviate from $H_I^{uncorrected}$ (indentation hardness H_I assuming a perfectly sharp Berkovich tip) at h_{max} of below about 400 nm. It is seen in Figure 13 that tip bluntness becomes important at shallow indentation depths; however, length scale dependent deformation in PMMA is still significant even after tip bluntness correction. Taking the effect of tip bluntness into account, indentation hardness of amorphous polymers PC, PS, and PMMA (including $H_I^{corrected}$ of Figure 13) is shown in Figure 14 where 10 s loading, holding, and unloading times together with strain rate of 0.1 s^{-1} were imposed in all indentation tests. Size effects are observed for all three polymers as indentation hardness (after correction for the tip bluntness) increases with decreasing indentation depth. High scatter in the experimental data is observed for all three polymers at shallow indentation depths below 100 nm indicating the presence of potential inaccuracies in the hardness determination at these small depths. Ignoring hardness data below 100 nm due to possible inaccuracies such as surface roughness, remarkable length scale dependent deformations are still observed at $h_{max} >$ 100 nm in all three polymers. Similarly, size effects in PC, PS, and PMMA can be observed in Figure 15 where the universal hardness (after correction for the tip bluntness) of these polymers, determined from the same experiments of Figure 13, is plotted over the indentation depth. Higher scatter in the data is again observed at small indentation depths $h_{max} >$ 100 nm. It should be noted that while size effects are clearly observed in PC, PS, and PMMA at depths of above 100 nm the indentation hardness of UHMWPE obtained from the same experiments of Figures 14

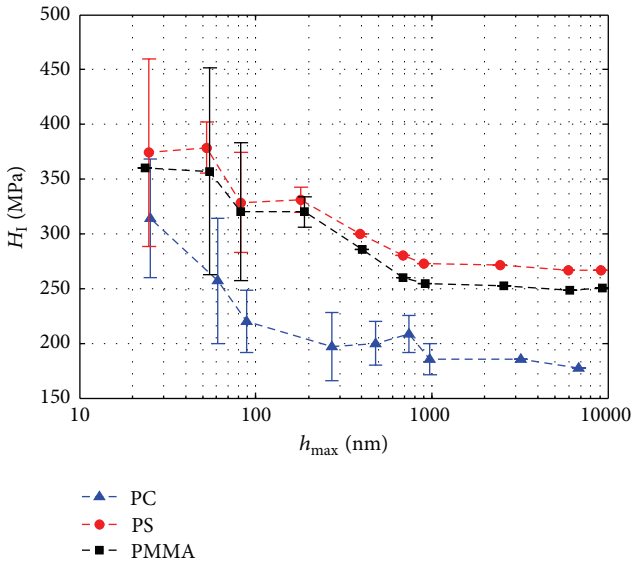

FIGURE 14: Indentation hardness of thermoplastic polymers obtained with 10 s loading, holding, and unloading times together with 0.1 s^{-1} strain rate [15].

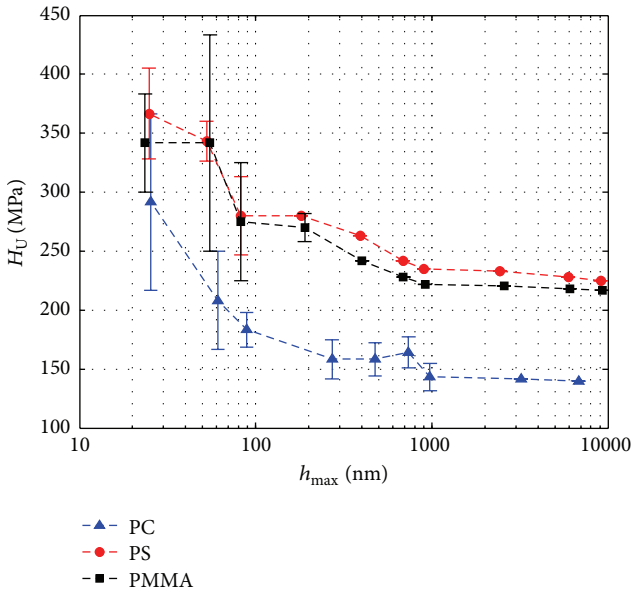

FIGURE 15: Universal hardness of thermoplastic polymers [15] obtained from the same experiments of Figure 14 (10 s loading, holding, and unloading times together with 0.1 s^{-1} strain rate).

and 15 does not show size effect for the same depth range (see Figure 2 where indentation hardness of UHMWPE remains almost constant).

Length scale dependent deformation of thermoplastic polymers is also observed in [28] where nanoindentation tests were performed by a Vicker tip at constant tip velocity during loading and unloading together with a 6 s holding time. The maximum applied force F_{max} varies from 0.2 to 300 mN where loading rate also increases from 0.14 to 70.61 mN/s with increasing F_{max}. Figure 16 shows indentation size effect

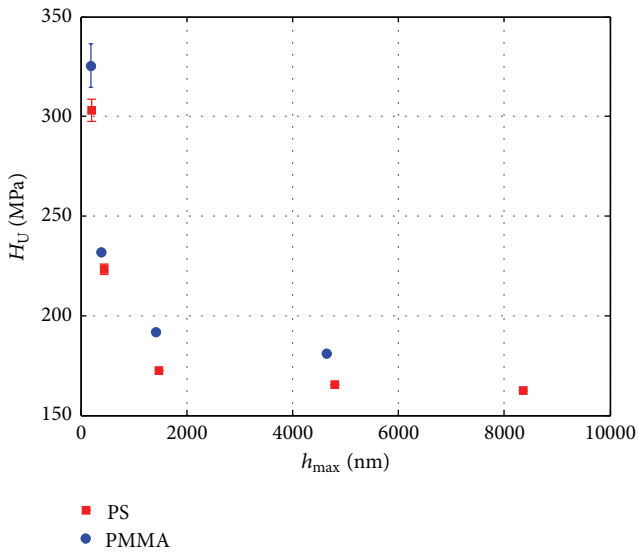

FIGURE 16: Universal hardness of thermoplastic polymers [28].

TABLE 2: $H_U^{0.2\,mN}/H_U^{bulk}$ ratio where $H_U^{0.2\,mN}$ and H_U^{bulk} are, respectively, the universal hardness at F_{max} = 0.2 mN and large indentation depths [28].

Sample	$H_U^{0.2\,mN}/H_U^{bulk}$
PS	1.84
SAN 1	1.79
SAN 2	1.73
PMMA 1	1.78
PMMA 2	1.77
PVC 1	1.60
PVC 2	1.57
PC	1.71

in PS and PMMA where universal hardness increases with decreasing h_{max} [28]. In addition to PS and PMMA, size effects were also observed in other amorphous thermoplastic polymers such as PC, PVC, and SAN where the hardness at shallow indentation depth (universal hardness at F_{max} = 0.2 mN) was found to be significantly higher than the bulk hardness (universal hardness at large indentation depths) [28]. The ratio of the universal hardness at F_{max} = 0.2 mN ($H_U^{0.2\,mN}$) to the bulk microhardness (H_U^{bulk}) is shown in Table 2 for different amorphous thermoplastic polymers of PS, PMMA, PC, PVC, and SAN. This ratio is around 1.8 for all glassy polymers of Table 2; however, for the more ductile polymer of PVC this ratio is slightly lower (about 1.6) [28]. The effect of material inhomogeneity (change in the material properties through thickness) and surface roughness on the size effect of polymers was also experimentally shown in [28]. In Figure 17, the universal hardness of PS is depicted as a function of indentation depth after 0.5, 1, and 5 μm of the top surface are removed. A significant decrease is observed in the hardness of PS after removing the top layers of the surface indicating a softening after surface removal. The softening was speculated in [28] to be attributed to a rough surface

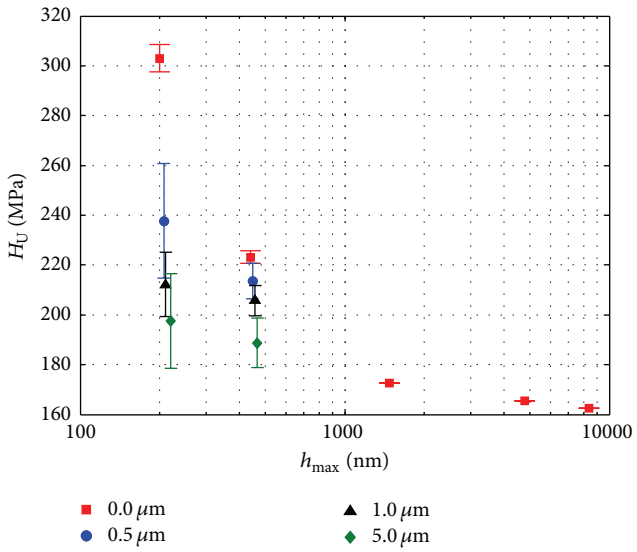

FIGURE 17: Universal hardness of PS when the first 0.5, 1, and 5 μm layers of the top surface are removed [28].

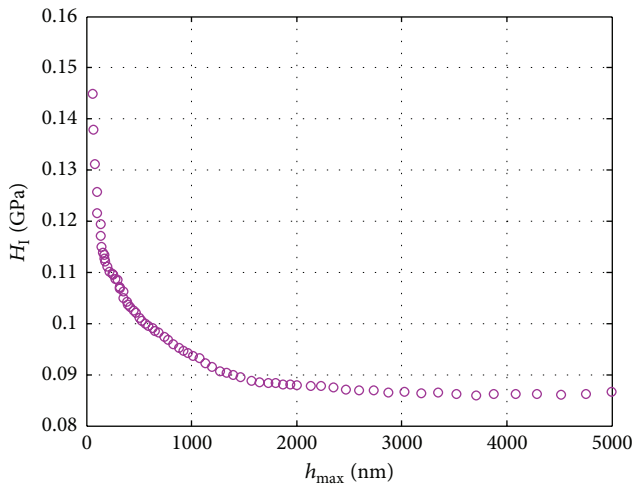

FIGURE 18: Indentation hardness of nylon 11 (PA11) obtained by a Berkovich tip and CSM method (a 0.05 s^{-1} strain rate is imposed during loading and unloading with a 60 s holding time) [63].

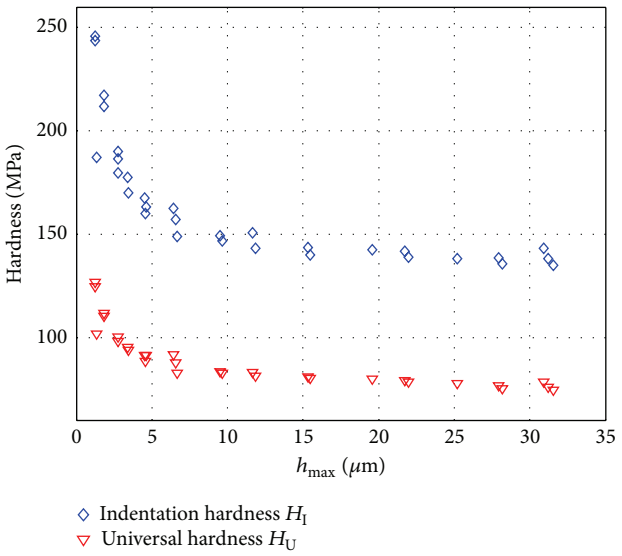

FIGURE 19: Indentation hardness H_I and universal hardness H_U of PAI obtained with a Berkovich tip with a 20 s loading and unloading times (without holding time) [64].

profile (compared to the smooth original surface) due to the cutting process.

Size effects were also observed in nylon 66 (PA66) by nanoindentation experiments with a Berkovich tip [39, 71, 72]. Nanoindentation tests were performed with a continuous stiffness measurement (CSM) approach as follows: loading segment with a constant strain rate of 0.05 s^{-1} to a depth of 5000 nm, a holding time of 60 s at the maximum applied force followed by unloading segment with the same rate of loading until 10% of the maximum applied force F_{max} is reached. The indentation size effect of PA66 is illustrated in Figure 2 where H_I increases with decreasing h_{max} at shallow indentation depths. As observed in [39], polishing does not significantly affect the hardness of PA66 depicted in Figure 2. The indentation size effect of PA66 was found to be unaffected by polishing as almost similar trends in the hardness were obtained for both polished and unpolished samples [39]. Performing nanoindentation tests with the same experimental details of PA66 [39, 71, 72], size effects were also experimentally observed in nylon 6 (PA6) [73–75] which exhibited a similar characteristic as observed in Figure 2 for PA66.

In addition to nylon 66 (PA66) [39, 71, 72] and nylon 6 (PA6) [73–75], length scale dependent deformation was also experimentally observed in nylon 11 (PA11) by nanoindentation testing with a Berkovich indenter tip [63]. As shown in Figure 18, indentation hardness of PA11 remarkably increases with decreasing indentation depth. The same experimental details of PA66 [39, 71, 72] mentioned above were also applied in the nanoindentation tests of PA11. However, compared to PA66 where size effect becomes significant at depths of around 200 nm, size effects in PA11 appear at larger indentation depths (at around $h_{max} \approx 2000$ nm) as shown in Figure 18.

Load-controlled indentations on polyamide-imide (PAI) with a Berkovich tip showed that size effect becomes significant at h_{max} below 10 μm [64]. Indentation hardness H_I and universal hardness H_U of PAI for an indentation depth range of about 30 to 1 μm are depicted in Figure 19 where 20 s loading and unloading times (without holding) were imposed in all tests [64].

Indentation hardness of glassy poly(ethylene terephthalate) (PET) obtained with a Vicker tip is shown in Figure 20 where a 6 s holding time was applied in all nanoindentation tests [61]. It is seen in Figure 20 that indentation hardness H_I is independent of indentation depth h_{max} at $h_{max} >$ 2000 nm. However, H_I of PET significantly increases with decreasing h_{max} at small indentation depths (see $H_I^{uncorrected}$

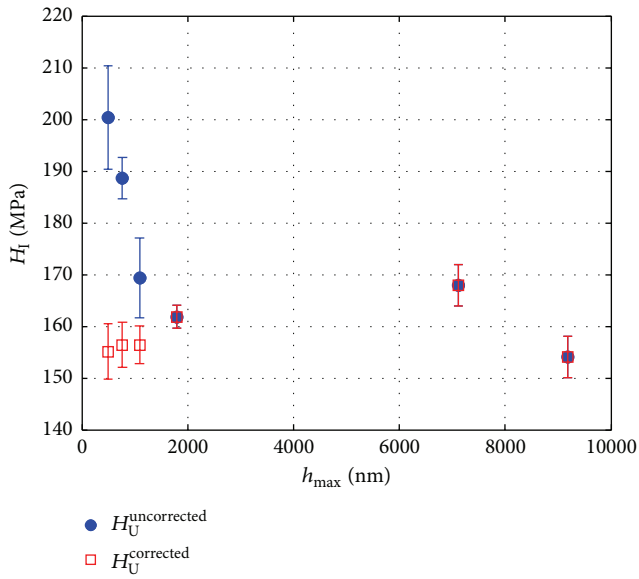

Figure 20: Indentation hardness of glassy poly(ethylene terephthalate) (PET) obtained with a Vicker tip ($H_I^{corrected}$ and $H_I^{uncorrected}$ represent the indentation hardness with and without considering the effect of tip bluntness, resp.) where a holding period of 6 s was used at the maximum applied force [61].

in Figure 20). This increase in the hardness of PET with decreasing indentation depth was attributed to indenter tip defects in [61] which will be later discussed in Section 3. Replacing the contact depth h_c of (2) with the corrected contact depth h_c' which includes tip bluntness, indentation hardness of PET is depicted in Figure 20 where hardness remains almost constant with indentation depth (see $H_I^{corrected}$ in Figure 20).

As mentioned above, indentation size effects become more pronounced in thermoset epoxy with increasing cross-link density [23]. Nanoindentation tests on thermoplastic PS with a Berkovich tip (with a tip curvature radius r = 50 nm) revealed that the indentation size effects increase with increasing molecular weight [58]. Six different polystyrene standards with molecular weights (M_p) of 4920, 10050, 19880, 52220, 96000, and 189300 g/mol were studied by nanoindentation testing [58] where 1.2 μm/min loading and unloading rates were imposed without holding time at peak load. Figure 21 demonstrates the indentation size effect of PS with M_p of 52220 g/mol as indentation hardness H_I determined by O&P method [53] increases with decreasing depth. The experimental hardness data of Figure 21 has been fitted with the theoretical hardness model of Nix and Gao [1]

$$H = H^* \sqrt{\frac{h^*}{h} + 1}, \tag{10}$$

where H^* is the hardness at infinite/macroscopic depth and h^* is a length scale parameter. As shown in Figure 22 and Table 3, the length scale parameter h^* increases with increasing molecular weights [58]. Such an increase in the length scale parameter h^* indicates that size effect in PS becomes more pronounced by increasing molecular weight. This change in the length scale parameter h^* with molecular weight is depicted in Figure 22 for M_p of 4920, 10050, 19880, and 52220 g/mol. As molecular length L increases with increasing molecular weights (see Table 3), it was concluded that h^* and subsequently the size effect in PS increase with increasing molecular length [58]. Note that in Figure 22 there is a sudden change in the slope of $h^* - M_p$ curve between 19880 and 52220 g/mol. A possible explanation for such a sudden change in Figure 22 might be associated with the degree of entanglement [58]. As shown in Figure 22, a critical molecular weight M_c = 36000 g/mol is reported for PS which can be associated with the minimum length of chains needed for generating chain entanglements. Polystyrene samples with molecular weights lower than M_c are characterized by few or no chain entanglement (PS samples with M_p of 4920, 10050, and 19880 g/mol), while polystyrene samples with molecular weights higher than M_c are characterized by considerable number of chain entanglement (PS sample with M_p of 52220 g/mol) which may influence the length scale dependent deformation of PS [58]. It should be mentioned that indentation tests on PS samples with high molecular weights (PS samples with M_p of 19880 and 52220 g/mol) provided highly scattered hardness data for which no length scale parameter (h^*) could be deduced [58]. As shown in Table 3, analogous to size effect in metals where h^*/b is constant (b is the Burgers vector) [58], the ratio h^*/R is almost constant in PS where R is the end-to-end distance (see [58] and references therein for further information about R). In addition to the Oliver and Pharr's method [53], a direct measurement method was also used to determine the indentation hardness of PS samples where the contact area of the sample at the maximum applied force was calculated by an atomic force microscope (AFM). The hardness data obtained from the direct measurement method, H_I^d, was found to be lower than the ones determined by Oliver and Pharr [53]. However, similar to the trend of H_I in Figure 21, a significant increase was observed in H_I^d (hardness of PS determined by the direct measurement method) with decreasing h_{max} illustrating the existence of length scale dependent deformation in PS [58].

Table 3: Molecular length L, end-to-end distance R, length scale parameter h^*, and h^*/R ratio of PS with different molecular weights M_p [58].

M_p (g/mol)	L (μm)	R (μm)	h^* (μm)	h^*/R
4920	0.015	0.0047	0.082	17
10050	0.030	0.0068	0.100	15
19880	0.059	0.0095	0.150	16
52220	0.150	0.0150	0.170	11

2.2.3. Elastomer/Rubber. Redrawn from [36], the indentation hardness of a silicon elastomer as a function of indentation depth is depicted in Figure 2. Comparing with the size effects observed in glassy polymers (both thermoset and thermoplastic) presented above, the size effects in the silicon elastomer [36] are more pronounced as the hardness increases

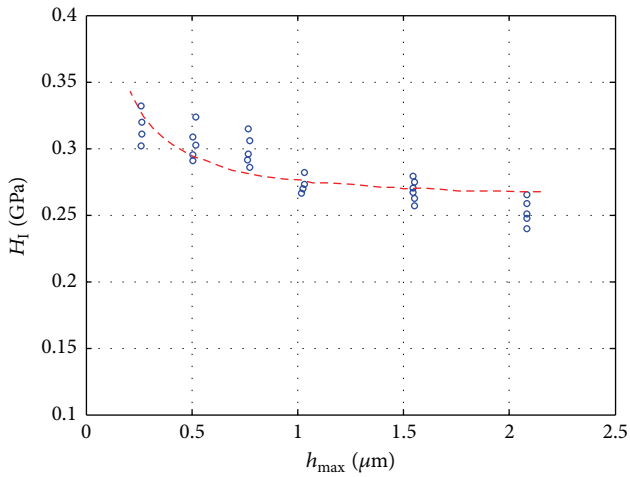

FIGURE 21: Indentation hardness of PS with molecular weights (M_p) of 52220 according to Oliver and Pharr method [53] obtained by a Berkovich tip with 1.2 μm/min loading and unloading rates and zero holding time [58].

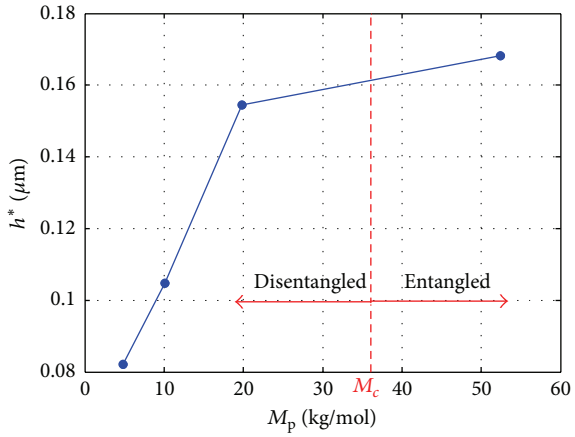

FIGURE 22: The length scale parameter h^* of (10) for PS with molecular weights of 4920, 10050, 19880, and 52220 g/mol [58].

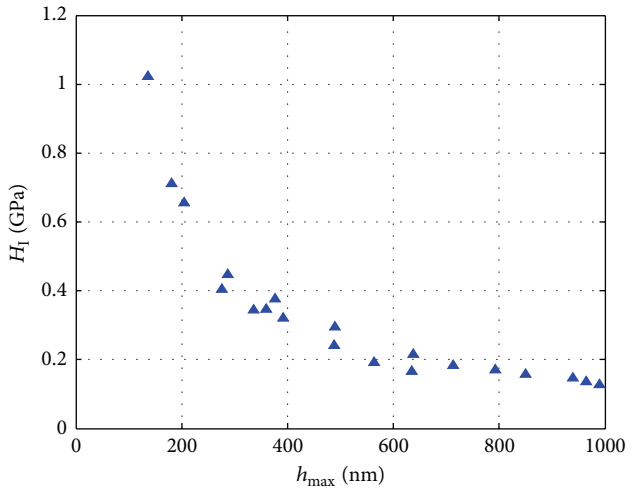

FIGURE 23: Indentation hardness of silicon elastomer determined with a Berkovich tip and the same loading and unloading rates of 150 μN/s [37].

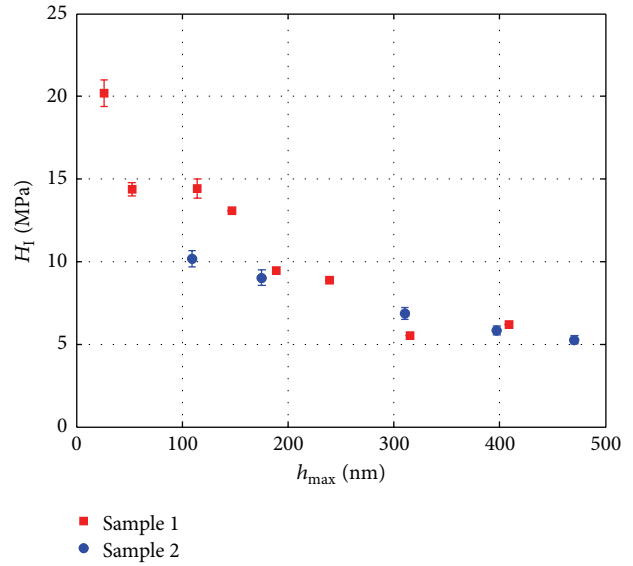

FIGURE 24: Indentation hardness of PDMS from two different samples obtained by a Berkovich tip with the same loading and unloading times of 40 s and a holding time of 3 s (each point represents ten indentations) [32].

by a factor of about seven with decreasing indentation depth from about 1500 to 200 nm. Such an amazing increase in the indentation hardness of silicon elastomer with decreasing depth is also reported in [37] which is redrawn in Figure 23. Nanoindentation tests were carried out by a Berkovich tip with constant loading and unloading rates of 150 μN/s where Oliver and Pharr's method [53] was adopted to determine the indentation hardness of Figure 23 [37].

Other nanoindentation studies reported in the literature on filled silicon rubber [38]; natural rubber [76] and PDMS [30–35] also show significant indentation size effects which are also considerably more pronounced than in thermoset and thermoplastic polymers. The size effects in PDMS can be observed in Figure 24 where H_I of two different samples of PDMS (prepared in the same way with 1 : 1 weight ratio of base agent to curing agent) is plotted with respect to h_{max} [32]. Each point in Figure 24 represents ten indentations carried out by a Berkovich tip with a curvature radius of about 100 nm [32]. Nanoindentation tests were performed with the same loading and unloading times of 40 s together with a 3 s holding time.

Similarly, indentation size effect in PDMS was observed in [33] where universal hardness H_U obtained by a sharp Berkovich tip was found to significantly increase with decreasing indentation depth from 5000 to 100 nm. Figure 25 illustrates the length scale dependent deformation of PDMS with 10% cross-link density by volume where H_U is determined with three loading times of 5, 20, and 80 s [33]. It is seen that size effect in PDMS is time independent for $h_{max} > 1000$ nm. However, H_U increases with decreasing loading time at shallow indentation depths $h_{max} < 1000$ nm

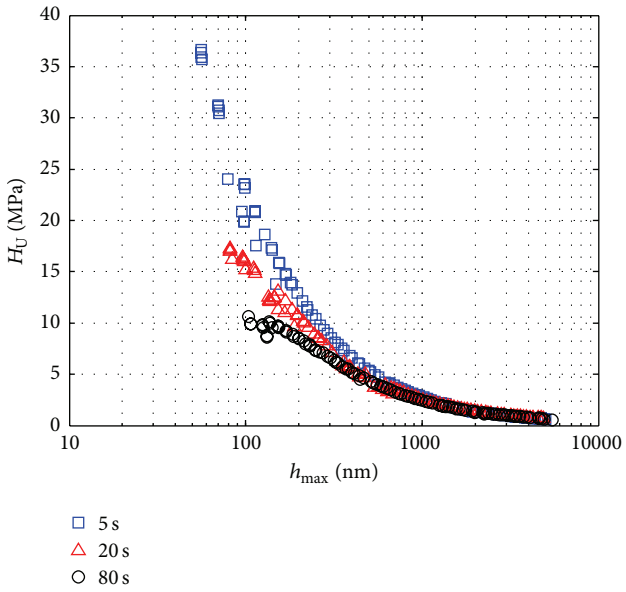

FIGURE 25: Universal hardness of PDMS determined by a Berkovich tip with different loading times of 5, 20, and 80 s [33].

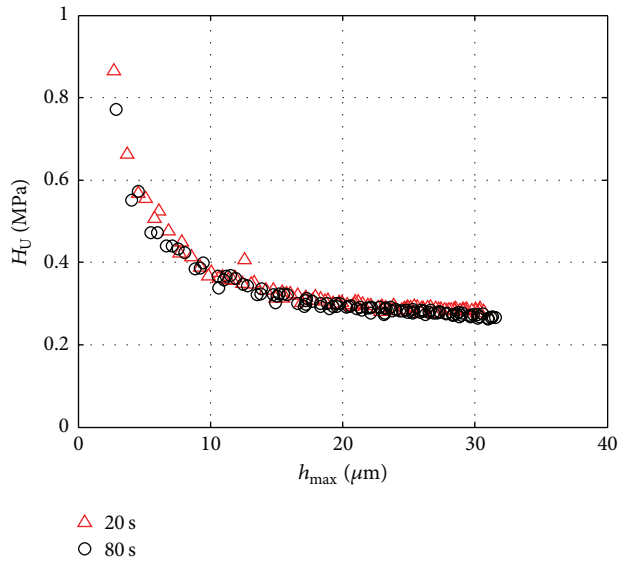

FIGURE 26: Universal hardness of PDMS determined by a Berkovich tip with different loading times of 20 and 80 s [59].

indicating time dependence of size effect in PDMS at small indentation depths [33]. In a recent study, indentation size effect of PDMS (with 10% cross-link density by volume) was investigated for an indentation depth of about 5 to 30 μm [59]. Universal hardness of PDMS determined with a Berkovich tip is shown in Figure 26 for two different loading times of 20 and 80 s [59]. It should be here mentioned that, similar to thermoset epoxy [23], size effect in PDMS was observed to increase with increasing cross-link density [34]. Performing indentation tests with a Vicker indenter tip on PDMS samples (with three different cross-link densities of 2.5%, 5%, and 10% by volume) showed that size effect in PDMS becomes more pronounced with increasing cross-link density [34]. As shown in [30, 33, 34, 59] and depicted in Figures 24–26, in addition to being significant, size effect in PDMS can be observed at very high indentation depths (indentation depth in which size effect in PDMS becomes significant was found to be dependent on the cross-link density of PDMS [34]). However, in contrast to [30, 33, 34, 59, 77], size effect in PDMS was only observed at small indentation depths $h_{max} < 200$ nm [78, 79] indicating that size effect in soft polymers is more complicated as it can be caused by various sources (such as surface detection or adhesion) which will be discussed later.

3. Origins of Indentation Size Effect in Polymers

In metals, size effect is usually considered to be associated with geometrically necessary dislocations arising from an increase in strain gradients related to nonuniform plastic deformation [1]. However, size effect characteristics in polymers are more complicated than metals as size effect in polymers has been also observed in elastic deformation [17, 18, 30, 33]. Also, in some polymers as in UHMWPE [15], size effects are essentially absent. Various explanations suggested as the origin of size effect in polymers will be reviewed in the following.

3.1. Higher Order Displacement Gradients. Similar to metals, where indentation size effect is considered to be associated with an increase in strain gradients with decreasing indentation depth [1, 4], size effects in polymers are also attributed to higher order gradients in the displacement [16, 17, 22–25, 29, 33, 49–51, 68]. The effects of higher order displacement gradients on the length scale dependent deformation of polymers were experimentally studied in [25] where the elastic modulus of epoxy was obtained by two indenter tips with different geometries: a Berkovich tip with a curvature radius $r < 40$ nm and a spherical tip with a radius of $R = 250\,\mu$m. Figure 27 depicts the elastic modulus of epoxy determined by the Berkovich tip, $E^{O\&P}$ (using Oliver and Pharr method [53], see (7)), and the spherical tip, E^{Hertz} (using Hertz theory [80]), where the elastic modulus E^{Hertz} is obtained by the Hertz contact theory

$$F = \frac{4}{3}\left(\frac{h}{R}\right)^{3/2} R^2 E_r^{Hertz} \tag{11}$$

in which F is the applied force, h the probing depth, R the radius of the sphere, and E_r^{Hertz} the reduced elastic modulus obtained from Hertz theory which is related to the elastic modulus of polymer, E^{Hertz}, via

$$\frac{1}{E_r^{Hertz}} = \frac{1-\nu^2}{E^{Hertz}} + \frac{1-\nu_i^2}{E_i}, \tag{12}$$

where, similar to (7), E_i and ν_i are, respectively, the elastic modulus and Poisson's ratio of indenter tip with ν being the Poisson's ratio of the polymer. As it is seen in Figure 27, the

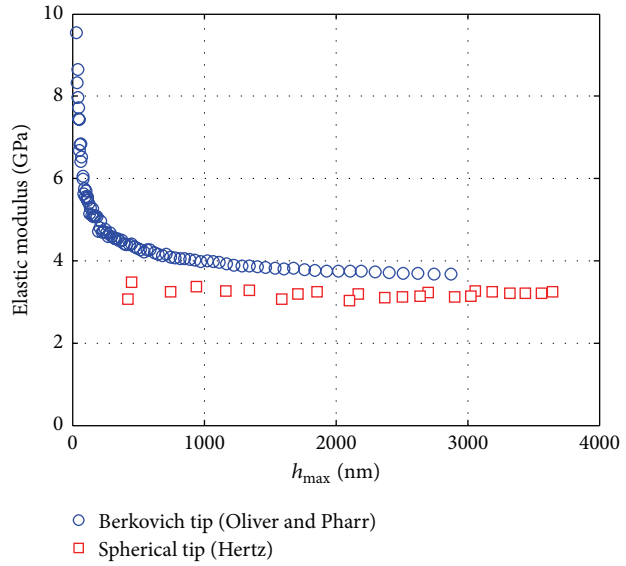

FIGURE 27: Elastic modulus of epoxy [25] determined with a Berkovich tip, $E^{O\&P}$, (using Oliver and Pharr method [53] with 20 s loading, holding, and unloading times) and with a spherical tip, E^{Hertz}, (using Hertz theory with 20 s loading time).

elastic modulus of epoxy obtained with the Berkovich tip, $E^{O\&P}$, increases with decreasing h_{max} while E^{Hertz} obtained by the spherical tip remains constant with h_{max} [25]. Such a different trend in the elastic modulus of epoxy determined by the Berkovich and spherical tips over the probing depths is attributed to the effect of higher order displacement gradients [25]. As shown in Figure 28, applying a sharp indenter tip, the higher order displacement gradients (strain gradients $\overline{\chi}$ in Figure 28) increase in magnitude with decreasing indentation depth, while these gradients remain essentially constant with h_{max} when a spherical tip is used [65, 66]. Note that, for a spherical tip, the strain gradient $\overline{\chi}$ is only dependent on the radius of tip, R, and is essentially independent of indentation depth as shown in Figure 28. Similar trends have been also observed in PDMS [59] where elastic modulus of PDMS determined by a Berkovich tip increases with h_{max}, while E^{Hertz} obtained from spherical tests remains almost constant with indentation depth. As illustrated in Figure 29, the elastic modulus of PDMS determined with a Berkovich tip ($E^{O\&P}$ and $E^{Sneddon}$ using O&P method and Sneddon's theory, resp.) increases with decreasing depth, while E^{Hertz} (applying Hertz theory) obtained with a spherical tip (with a radius of 250 μm) does not change with indentation depth. For elastic materials and a conical tip, $E^{Sneddon}$ [81] for frictionless indentation can be obtained by Sneddon's theory via the following load-displacement relation:

$$F = \frac{2\tan(\alpha)\,E^{Sneddon}}{\pi\left(1-\nu^2\right)}h^2, \tag{13}$$

where $\alpha = 70.3^\circ$ is the half angle defining a cone equivalent to a Berkovich tip. It should be here mentioned that, similar to Figures 27 and 29, Swadener et al. [2] observed different trends for the hardness of metals determined by Berkovich and spherical tips. Similar to the present finding in epoxy and PDMS, it was shown that, for metals, hardness determined with a Berkovich tip increases with decreasing h_{max} whereas hardness is independent of indentation depth when a spherical tip is used [2].

As classical elastoplastic theories do not take the effects of higher order displacement gradients into account, length scale dependent deformation of polymers presented above cannot be predicted by these local classical theories. To capture the abovementioned size effect in polymers, few theoretical models have been developed where size effect of polymers is attributed to the effect of higher order displacement gradients at micro to submicro scales.

Based on a molecular kinking mechanism and the molecular theory of yielding of glassy polymers, a strain gradient plasticity law was developed in [16, 22] where a molecular and temperature dependent strain gradient plasticity parameter was proposed and related to indentation hardness. A theoretical indentation hardness model

$$H = H_*\left(1+\sqrt{\frac{h_*}{h}}\right) \tag{14}$$

was proposed in [16, 22] which shows good agreement with the experimental hardness data of the thermoset epoxy and the thermoplastic PC [16] depicted in Figure 2 where H_* is the hardness at infinite depth and h_* is a constant dependent on material behavior and temperature [16, 22]. A strain gradient plasticity was suggested in [16, 22] which was incorporated into a viscoelastic-plastic constitutive model of [82] to predict size effect of glassy polymers observed in nanoindentation experiments [51]. Finite element simulation results demonstrated that higher order gradients of displacement should be incorporated into constitutive model to capture the length scale dependent deformation of glassy polymers in micro/nanoindentations [51].

Another higher order displacement gradients based model was developed in [49] where size effect in elastic deformation of polymers was attributed to rotation gradients effects arising from finite bending stiffness of polymer chains and their interactions. To account for the effect of higher order gradients of displacement on the deformation mechanism of polymers, the local elastic deformation energy density W_ε^e is augmented by a nonlocal rotation gradients term W_χ yielding the total elastic deformation energy density W [49]

$$W = W_\varepsilon^e + W_\chi = \frac{1}{2}\varepsilon_{ij}C_{ijkl}\epsilon_{kl} + \frac{\widetilde{K}}{3}\chi_{ij}^S\chi_{ij}^S, \tag{15}$$

where ε_{ij} is the infinitesimal strain tensor, C_{ijkl} is the elasticity tensor, and $\widetilde{K}$ is a material constant (see [49] where $\widetilde{K}$ is micromechanically motivated). Following couple stress elasticity theory of [83], it is seen in (15) that only the symmetric part of the rotation gradient

$$\chi_{ij}^S = \frac{1}{2}\left(\chi_{ij}+\chi_{ji}\right) = \frac{1}{2}\left(\omega_{i,j}+\omega_{j,i}\right) \tag{16}$$

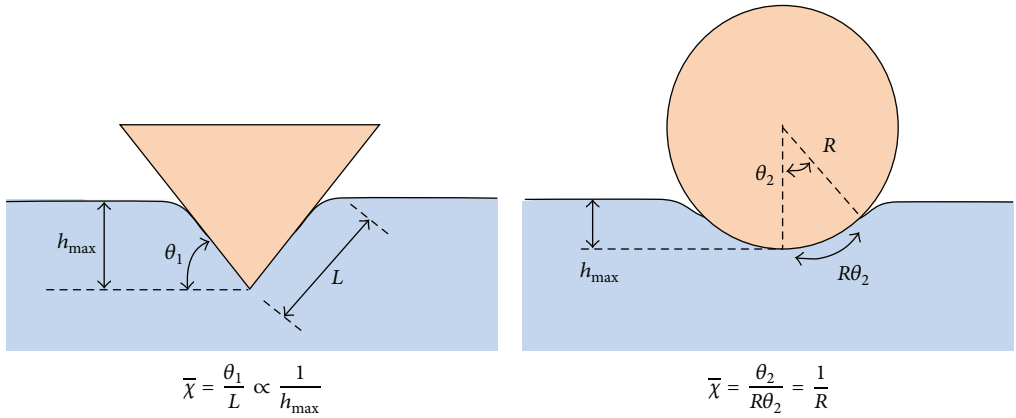

FIGURE 28: Dependence of strain gradient $\overline{\chi}$ on h_{max} for different tip geometries [65, 66].

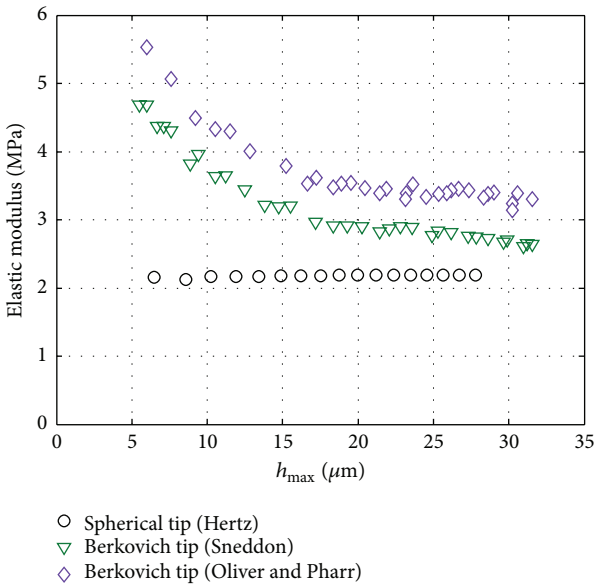

FIGURE 29: Elastic modulus of PDMS [59] determined with loading and unloading times of 80 s (without holding time).

is assumed to contribute to the total elastic deformation energy density W (more specifically to W_χ in (15)), where the symmetric part of the rotation gradient tensor χ_{ij}^{S} in (16) can be either defined by the rotation gradient tensor

$$\chi_{ij} = \frac{1}{2} e_{inm} u_{m,jn} \tag{17}$$

or the infinitesimal rotation vector

$$\omega_i = \frac{1}{2} e_{imn} u_{n,m}, \tag{18}$$

where u_i, $u_{i,j}$, and e_{imn} are the displacement vector, displacement gradients, and permutation symbol, respectively [49]. The abovementioned rotation gradient based elastic formulation was extended in [50] to include inelastic deformation and a theoretical hardness model was developed

$$H = H_0 \left(1 + \frac{c_\ell}{h}\right), \tag{19}$$

where, similar to H_* in (14), H_0 is the hardness at infinite/macroscopic depth and c_ℓ is the material length scale parameter which has been micromechanically motivated in [50]. The theoretical hardness model (19) showed good agreement with the experimental hardness data of PC [68], epoxy [25, 68], PS [68], PAI [68], PA66 [68], PMMA [68], and PDMS [33]. Based on the hardness model (19), a theoretical stiffness model

$$K = H_0 C \left(c_\ell + 2h\right) \tag{20}$$

was proposed by Alisafaei et al. [25] where the parameters H_0 and c_ℓ are obtained by fitting the hardness model (19) to the experimental hardness data and C is a constant equal to 26.43 for Berkovich tip. The theoretical stiffness model (20) was compared with the experimental stiffness, K_m, of epoxy [25] and PDMS [33] obtained from nanoindentation tests. K_m is obtained by calculating the derivative of force F with respect to indentation depth h at the last data point of loading curve (point B in Figure 1(a)) [25, 33]. In Figures 30 and 31, the theoretical stiffness model (20) is compared with the experimental data of K_m obtained for PDMS [33] and epoxy [25], respectively. As demonstrated in Figures 30 and 31, good agreement is found between the experimental stiffness data of PDMS and epoxy with the theoretical stiffness model (20) corroborating the validity of the hardness model (19) to predict the size effects in elastomer PDMS and thermoset epoxy. It is seen in Figures 30 and 31 that, unlike materials which do not exhibit size effect, K_m experimentally determined for PDMS and epoxy do not approach zero when $h_{max} \to 0$. This trend observed in the experimental stiffness K_m is consistent with the theoretical stiffness model (20) which predicts a nonzero value of the stiffness ($K = c_\ell H_0 C$) when $h_{max} \to 0$. For materials which do not show size effect ($c_\ell = 0$), the theoretical stiffness model (20) predicts a linear relation between the stiffness K and indentation depth h ($K = 2H_0 Ch$) which is consistent with experimental stiffness data of fused silica in [25, 33] (size effect in fused silica is known to be not pronounced [84]).

In addition to the two higher order displacement gradient based theories [22, 49] mentioned above, extending the mechanism based theories of crystalline metals, Voyiadjis

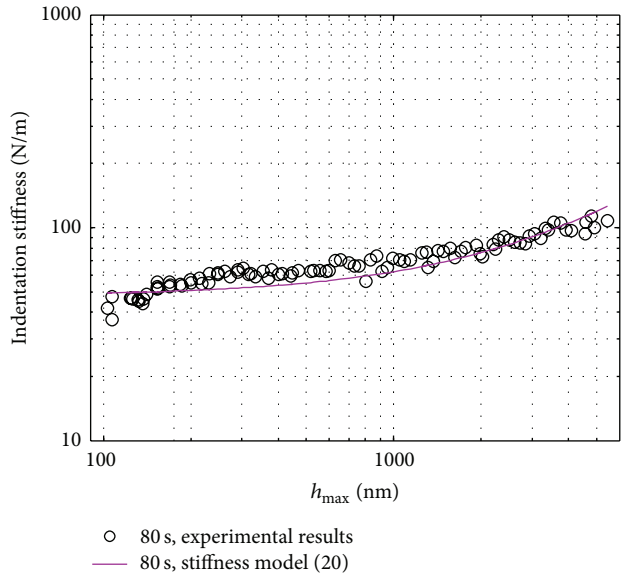

FIGURE 30: Comparison of the experimental stiffness K_m of PDMS obtained with a Berkovich tip with the indentation stiffness model (20) where 80 s loading time was used in nanoindentation experiments [33].

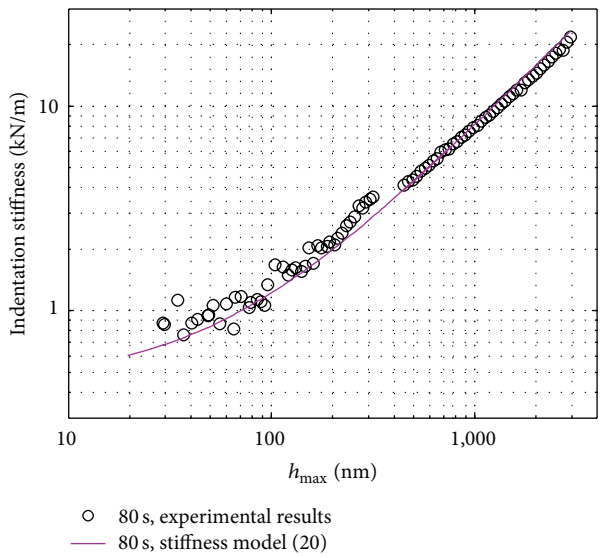

FIGURE 31: Comparison of the experimental stiffness K_m of epoxy obtained with a Berkovich tip with the indentation stiffness model (20) where 80 s loading time was used in nanoindentation experiments [25].

et al. [29] recently developed a strain gradient plasticity formulation for semicrystalline polymers in which size effects in semicrystalline polymers were attributed to crystalline subphase embedded within an amorphous matrix. Two kink mechanisms of grounded kink and active kink were considered to, respectively, capture nonlocalized effects (e.g., uniform plastic deformation) and localized effects (viscoplastic deformation effects induced by nonuniform slippage mechanisms, e.g., localized plastic deformation which is found in indentation tests around a sharp indenter tip). Utilizing a Cosserat continuum formulation and adopting considerations in [49], size effects in amorphous polymers were also elaborately modeled in [29] where a flow rule was proposed for amorphous polymers. Furthermore, a theoretical hardness model was developed

$$\left(\frac{H}{H'}\right)^{\beta} = 1 + \left(\frac{h'}{h}\right)^{\beta/2}, \tag{21}$$

where, similar to (10), (14), and (19), H' is the hardness at infinite depth (microhardness of material which is determined in the absence of size effect), β is the tip geometry correction factor represented in (6) and defined in Table 1, and h' is a material constant which is related to the material length scale [29].

It may be worth noting that for the material model of (15) to (18), a finite element procedure has been developed in [85, 86] with which two-dimensional numerical simulations have been performed in [87] to study stiffening effects in reinforced polymer composites with decreasing reinforcement sizes [21]. Similar to the experimental results [21], numerical simulations of [87] showed stiffening of reinforced polymer composites with decreasing reinforcement size at high fiber volume fractions.

3.1.1. Influence of Molecular Structure on ISE. As discussed in Section 2, size effects in elastomers are considerably more pronounced than in plastic polymers (thermoset and thermoplastic polymers). However, as shown in Figure 2, the characteristics of size effects even in thermoset and thermoplastic polymers were found to differ for different polymers. The characteristics of size effect in thermoset and thermoplastic polymers were attributed to molecular structures of these polymers [68] which are discussed here.

Depth Dependent Hardness of Polymers with Aromatic Components. Indentation size effect of PC [16] shown in Figure 2 is redrawn in Figure 32 together with a sequence of its molecular structure [68] and the theoretical hardness model (19) where $H_0 = 0.165$ GPa and $c_\ell = 0.0442\,\mu$m. It is seen that there is excellent agreement between the experimental hardness data of PC and the theoretical hardness model (19). Such a strong indentation size effect observed at large indentation depths is also observed in epoxy, PS, and PAI where all these polymers contain aromatic components (see [68] for their molecular structures) and their experimental hardness data show excellent agreement with the hardness model (19).

Depth Dependent Hardness of Polymers without Aromatic Components. Indentation hardness of UHMWPE as a function of h_{max} depicted in Figure 2 is redrawn in Figure 33 as well as a sequence of its molecular structure [68]. As mentioned in Section 2 and shown in Figure 33, UHMWPE does not exhibit any significant indentation size effect even at shallow indentation depths $h_{max} < 50$ nm. As demonstrated in Figure 33, unlike the abovementioned polymers with aromatic components, UHMWPE has a homogenous

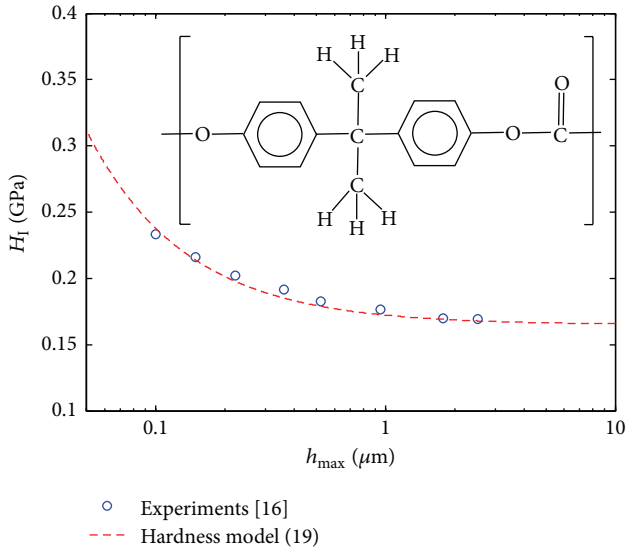

FIGURE 32: Indentation hardness of PC [16] and its molecular structure [68].

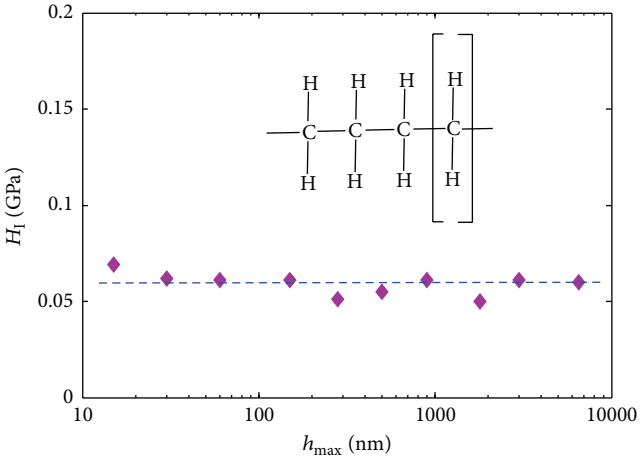

FIGURE 33: Indentation hardness of UHMWPE [15] and its molecular structure [68].

and highly flexible molecular structure. Similar trend can be observed in PTFE [69] where indentation hardness H_I remains constant with indentation depth indicating that PTFE does not show any indentation size effects at an indentation depth range of about 2000 to 20 nm. Note that, similar to UHMWPE shown in Figure 33, PTFE has a homogenous and highly flexible molecular structure without any aromatic components (see [68]). Indentation size effect of PA66 [39] presented in Figure 2 is also depicted in Figure 34 along with the hardness model (19) with $H_0 = 0.0905$ GPa and $c_\ell = 0.0276\,\mu$m. Compared to UHMWPE and PTFE, PA66 has a more complex molecular structure (see Figures 33 and 34) and shows indentation size effect at smaller indentation depths (compared to those polymers which contain aromatic components) [68].

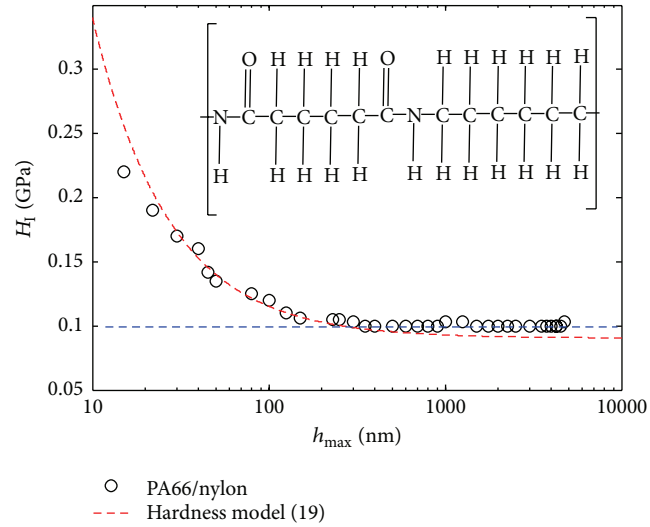

FIGURE 34: Indentation size effect of PA66 [39] and its molecular structure [68].

3.2. Surface Effect, Friction, Tip Imperfection, and Material Inhomogeneity. In addition to the abovementioned higher order displacement gradient based models, there are also other explanations suggested as the origin of size effect in polymers including change in the material properties through thickness [15], friction [34], surface effects [36, 52], tip imperfection [61], adhesion, and others. Unlike in indentation size effects in metals, where the elastic modulus remains constant with depth, elastic moduli of polymers were found to increase with decreasing indentation depth. As illustrated in Figure 27, elastic modulus $E^{O\&P}$ of thermoset epoxy determined by a Berkovich tip increases with decreasing indentation depth. Corresponding to Figures 14 and 15, elastic modulus $E^{O\&P}$ of thermoplastic polymers PC, PS, and PMMA, obtained from the same experiments of Figures 14 and 15, increases with decreasing indentation depth (see Figure 35). In addition to thermoplastic polymers PC, PS, and PMMA mentioned above, elastic moduli of other thermoplastic polymers PA66 [39], PMR-15 [40], and PA6 [41] were also found to increase with decreasing h_{max} (however, opposite to the abovementioned trend for $E^{O\&P}$ of thermoplastic polymers, elastic modulus $E^{O\&P}$ of PS in [58] was reported to be independent of indentation depth). In addition to thermoset and thermoplastic polymers, elastic modulus of PDMS elastomer was also shown to increase with decreasing indentation depth [30, 59]. As demonstrated in Figure 29, elastic modulus of PDMS obtained by a Berkovich tip ($E^{O\&P}$ and $E^{Sneddon}$ using O&P method and Sneddon's theory, resp.) increases as h_{max} decreases [59]. Similarly, in a careful elaborated nanoindentation experiments with a Berkovich tip [30], elastic modulus of PDMS shown in Figure 36 was found to significantly increase with decreasing indentation depth indicating the existence of size effect in elastomers. A straightforward possible explanation for such a change in the elastic modulus can be changes in the material properties through the depth of the polymer [15].

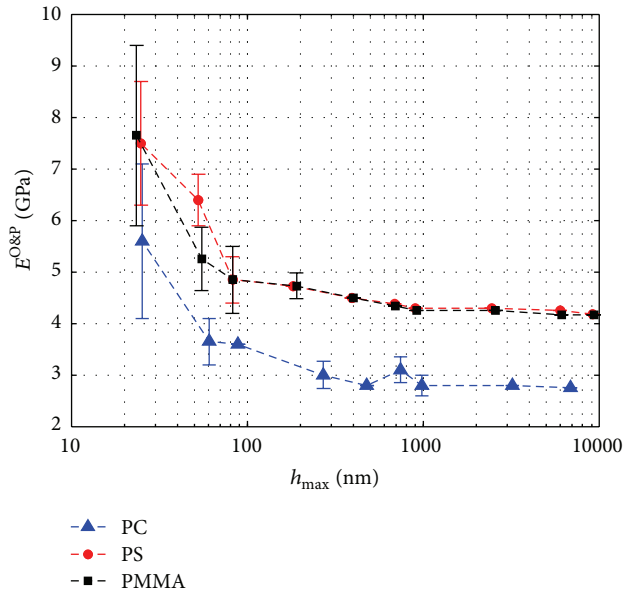

Figure 35: Elastic modulus of thermoplastic polymers according to Oliver and Pharr method [53] obtained with 10 s loading, holding, and unloading times together with 0.1 s^{-1} strain rate [15].

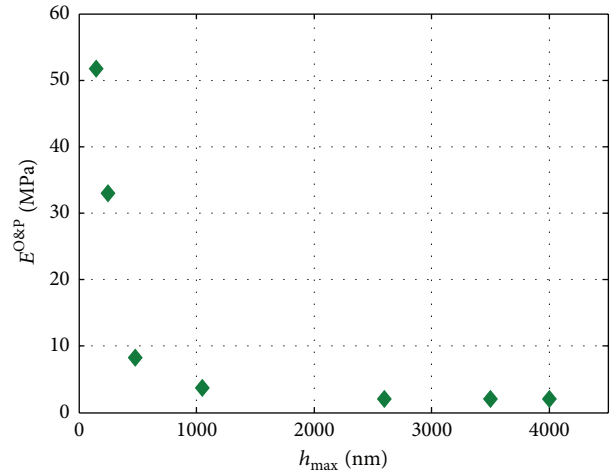

Figure 36: Elastic modulus of PDMS (with 15% cross-link density by weight) determined by a Berkovich tip [30].

However, in [25, 59, 76] it has been argued that such material inhomogeneities (changes in the material properties through the depth) cannot be the only source of indentation size effect in polymers as the measured elastic moduli of epoxy and PDMS obtained by a spherical tip (E^{Hertz}, resp., presented in Figures 27 and 29) stay constant with h_{max} while the elastic moduli determined by a sharp Berkovich tip increase with decreasing indentation depth. The influences of material inhomogeneity and surface roughness on the size effect of polymers have been investigated in [28] where a significant decrease in the hardness of PS was observed by removing the top surface as shown in Figure 17. However, the hardness of PS still increases with decreasing h_{max}, even after removing the top layers of the surface, indicating that material inhomogeneity and surface roughness cannot be the only source of length scale dependent deformation in polymers. Furthermore, studying the effects of material inhomogeneity on the size effect of epoxy [17] revealed that the significant increase in the bending rigidity of epoxy microbeams is not associated with the presence of stiff surface layers. Considering material inhomogeneity, it should be mentioned that certain sample fabrication/processing methods may induce structural inhomogeneity that may even result in anisotropic behavior of the polymer sample [88].

In addition to the material inhomogeneity, surface effect/stress and surface roughness are also known to be among the factors that cause indentation size effect at shallow indentation depths [36, 52]. There exists a critical indentation depth below which surface effect plays an important role on the length scale dependent deformation of polymers [36]. Adhesion [89–94] is also another factor that can cause indentation size effect particularly at small indentation depths of soft polymers [59, 60].

Conflict of Interests

The authors declare that there is no conflict of interests regarding the publication of this paper.

Acknowledgment

The material of this paper is based on work supported by the U.S. National Science Foundation under Grants no. 1102764 and no. 1126860.

References

[1] W. D. Nix and H. Gao, "Indentation size effects in crystalline materials: a law for strain gradient plasticity," *Journal of the Mechanics and Physics of Solids*, vol. 46, no. 3, pp. 411–425, 1998.

[2] J. G. Swadener, E. P. George, and G. M. Pharr, "The correlation of the indentation size effect measured with indenters of various shapes," *Journal of the Mechanics and Physics of Solids*, vol. 50, no. 4, pp. 681–694, 2002.

[3] R. K. Abu Al-Rub, "Prediction of micro and nanoindentation size effect from conical or pyramidal indentation," *Mechanics of Materials*, vol. 39, no. 8, pp. 787–802, 2007.

[4] G. Feng and W. D. Nix, "Indentation size effect in MgO," *Scripta Materialia*, vol. 51, no. 6, pp. 599–603, 2004.

[5] A. A. Elmustafa and D. S. Stone, "Indentation size effect in polycrystalline F.C.C. metals," *Acta Materialia*, vol. 50, no. 14, pp. 3641–3650, 2002.

[6] R. K. Abu Al-Rub and G. Z. Voyiadjis, "Analytical and experimental determination of the material intrinsic length scale of strain gradient plasticity theory from micro- and nano-indentation experiments," *International Journal of Plasticity*, vol. 20, no. 6, pp. 1139–1182, 2004.

[7] Q. Ma and D. R. Clarke, "Size dependent hardness of silver single crystals," *Journal of Materials Research*, vol. 10, no. 4, pp. 853–863, 1995.

[8] C. Motz, T. Schöberl, and R. Pippan, "Mechanical properties of micro-sized copper bending beams machined by the focused ion beam technique," *Acta Materialia*, vol. 53, no. 15, pp. 4269–4279, 2005.

[9] N. A. Fleck, G. M. Muller, M. F. Ashby, and J. W. Hutchinson, "Strain gradient plasticity: theory and experiment," *Acta Metallurgica et Materialia*, vol. 42, no. 2, pp. 475–487, 1994.

[10] L. Tsagrakis and E. C. Aifantis, "Recent developments in gradient plasticity. Part I. Formulation and size Effects," *Journal of Engineering Materials and Technology*, vol. 124, no. 3, pp. 352–357, 2002.

[11] M. B. Taylor, H. M. Zbib, and M. A. Khaleel, "Damage and size effect during superplastic deformation," *International Journal of Plasticity*, vol. 18, no. 3, pp. 415–442, 2002.

[12] Y. Cao, S. Allameh, D. Nankivil, S. Sethiaraj, T. Otiti, and W. Soboyejo, "Nanoindentation measurements of the mechanical properties of polycrystalline Au and Ag thin films on silicon substrates: effects of grain size and film thickness," *Materials Science and Engineering A*, vol. 427, no. 1-2, pp. 232–240, 2006.

[13] Y. W. Yan, L. Geng, and A. B. Li, "Experimental and numerical studies of the effect of particle size on the deformation behavior of the metal matrix composites," *Materials Science and Engineering A*, vol. 448, no. 1-2, pp. 315–325, 2007.

[14] Z. Xue, Y. Huang, and M. Li, "Particle size effect in metallic materials: a study by the theory of mechanism-based strain gradient plasticity," *Acta Materialia*, vol. 50, no. 1, pp. 149–160, 2002.

[15] B. J. Briscoe, L. Fiori, and E. Pelillo, "Nano-indentation of polymeric surfaces," *Journal of Physics D: Applied Physics*, vol. 31, no. 19, pp. 2395–2405, 1998.

[16] A. C. M. Chong and D. C. C. Lam, "Strain gradient plasticity effect in indentation hardness of polymers," *Journal of Materials Research*, vol. 14, no. 10, pp. 4103–4110, 1999.

[17] D. C. C. Lam, F. Yang, A. C. M. Chong, J. Wang, and P. Tong, "Experiments and theory in strain gradient elasticity," *Journal of the Mechanics and Physics of Solids*, vol. 51, no. 8, pp. 1477–1508, 2003.

[18] A. W. McFarland and J. S. Colton, "Role of material microstructure in plate stiffness with relevance to microcantilever sensors," *Journal of Micromechanics and Microengineering*, vol. 15, no. 5, pp. 1060–1067, 2005.

[19] A. Arinstein, M. Burman, O. Gendelman, and E. Zussman, "Effect of supramolecular structure on polymer nanofibre elasticity," *Nature Nanotechnology*, vol. 2, no. 1, pp. 59–62, 2007.

[20] L. Sun, R. P. S. Han, J. Wang, and C. T. Lim, "Modeling the size-dependent elastic properties of polymeric nanofibers," *Nanotechnology*, vol. 19, no. 45, Article ID 455706, 2008.

[21] S.-Y. Fu, X.-Q. Feng, B. Lauke, and Y.-W. Mai, "Effects of particle size, particle/matrix interface adhesion and particle loading on mechanical properties of particulate-polymer composites," *Composites Part B: Engineering*, vol. 39, no. 6, pp. 933–961, 2008.

[22] D. C. C. Lam and A. C. M. Chong, "Indentation model and strain gradient plasticity law for glassy polymers," *Journal of Materials Research*, vol. 14, no. 9, pp. 3784–3788, 1999.

[23] D. C. C. Lam and A. C. M. Chong, "Effect of cross-link density on strain gradient plasticity in epoxy," *Materials Science and Engineering: A*, vol. 281, no. 1-2, pp. 156–161, 2000.

[24] D. C. C. Lam and A. C. M. Chong, "Characterization and modeling of specific strain gradient modulus of epoxy," *Journal of Materials Research*, vol. 16, no. 2, pp. 558–563, 2001.

[25] F. Alisafaei, C.-S. Han, and N. Lakhera, "Characterization of indentation size effects in epoxy," *Polymer Testing*, vol. 40, pp. 70–75, 2014.

[26] A. K. Dutta, D. Penumadu, and B. Files, "Nanoindentation testing for evaluating modulus and hardness of single-walled carbon nanotube–reinforced epoxy composites," *Journal of Materials Research*, vol. 19, no. 1, pp. 158–164, 2004.

[27] M. Sánchez, J. Rams, M. Campo, A. Jiménez-Suárez, and A. Ureña, "Characterization of carbon nanofiber/epoxy nanocomposites by the nanoindentation technique," *Composites Part B: Engineering*, vol. 42, no. 4, pp. 638–644, 2011.

[28] F. J. B. Calleja, A. Flores, and G. H. Michler, "Microindentation studies at the near surface of glassy polymers: influence of molecular weight," *Journal of Applied Polymer Science*, vol. 93, no. 4, pp. 1951–1956, 2004.

[29] G. Z. Voyiadjis, A. Shojaei, and N. Mozaffari, "Strain gradient plasticity for amorphous and crystalline polymers with application to micro- and nano-scale deformation analysis," *Polymer*, vol. 55, no. 16, pp. 4182–4198, 2014.

[30] C. A. Charitidis, "Nanoscale deformation and nanomechanical properties of polydimethylsiloxane (PDMS)," *Industrial & Engineering Chemistry Research*, vol. 50, no. 2, pp. 565–570, 2011.

[31] C. Charitidis, "Nanoscale deformation and nanomechanical properties of soft matter study cases: polydimethylsiloxane, cells and tissues," *ISRN Nanotechnology*, vol. 2011, Article ID 719512, 13 pages, 2011.

[32] E. P. Koumoulos, P. Jagdale, I. A. Kartsonakis, M. Giorcelli, A. Tagliaferro, and C. A. Charitidis, "Carbon nanotube/polymer nanocomposites: a study on mechanical integrity through nanoindentation," *Polymer Composites*, 2014.

[33] F. Alisafaei, C.-S. Han, and S. H. R. Sanei, "On the time and indentation depth dependence of hardness, dissipation and stiffness in polydimethylsiloxane," *Polymer Testing*, vol. 32, no. 7, pp. 1220–1228, 2013.

[34] Y. Y. Lim and M. M. Chaudhri, "Indentation of elastic solids with a rigid Vickers pyramidal indenter," *Mechanics of Materials*, vol. 38, no. 12, pp. 1213–1228, 2006.

[35] A. J. Wrucke, C.-S. Han, and P. Majumdar, "Indentation size effect of multiple orders of magnitude in polydimethylsiloxane," *Journal of Applied Polymer Science*, vol. 128, no. 1, pp. 258–264, 2013.

[36] T.-Y. Zhang and W.-H. Xu, "Surface effects on nanoindentation," *Journal of Materials Research*, vol. 17, no. 7, pp. 1715–1720, 2002.

[37] W.-H. Xu, Z.-Y. Xiao, and T.-Y. Zhang, "Mechanical properties of silicone elastomer on temperature in biomaterial application," *Materials Letters*, vol. 59, no. 17, pp. 2153–2155, 2005.

[38] R. V. S. Tatiraju and C.-S. Han, "Rate dependence of indentation size effects in filled silicone rubber," *Journal of Mechanics of Materials and Structures*, vol. 5, no. 2, pp. 277–288, 2010.

[39] L. Shen, T. Liu, and P. Lv, "Polishing effect on nanoindentation behavior of nylon 66 and its nanocomposites," *Polymer Testing*, vol. 24, no. 6, pp. 746–749, 2005.

[40] Y. C. Lu, D. C. Jones, G. P. Tandon, S. Putthanarat, and G. A. Schoeppner, "High temperature nanoindentation of PMR-15 polyimide," *Experimental Mechanics*, vol. 50, no. 4, pp. 491–499, 2010.

[41] R. Seltzer, J.-K. Kim, and Y.-W. Mai, "Elevated temperature nanoindentation behaviour of polyamide 6," *Polymer International*, vol. 60, no. 12, pp. 1753–1761, 2011.

[42] J. F. Nye, "Some geometrical relations in dislocated crystals," *Acta Metallurgica*, vol. 1, no. 2, pp. 153–162, 1953.

[43] A. Arsenlis and D. M. Parks, "Crystallographic aspects of geometrically-necessary and statistically-stored dislocation density," *Acta Materialia*, vol. 47, no. 5, pp. 1597–1611, 1999.

[44] N. A. Fleck and J. W. Hutchinson, "A phenomenological theory for strain gradient effects in plasticity," *Journal of the Mechanics and Physics of Solids*, vol. 41, no. 12, pp. 1825–1857, 1993.

[45] H. Gao, Y. Huang, W. D. Nix, and J. W. Hutchinson, "Mechanism-based strain gradient plasticity—I. Theory," *Journal of the Mechanics and Physics of Solids*, vol. 47, no. 6, pp. 1239–1263, 1999.

[46] C.-S. Han, H. Gao, Y. Huang, and W. D. Nix, "Mechanism-based strain gradient crystal plasticity—I. Theory," *Journal of the Mechanics and Physics of Solids*, vol. 53, no. 5, pp. 1188–1203, 2005.

[47] Y. Huang, S. Qu, K. C. Hwang, M. Li, and H. Gao, "A conventional theory of mechanism-based strain gradient plasticity," *International Journal of Plasticity*, vol. 20, no. 4-5, pp. 753–782, 2004.

[48] Y. Huang, Z. Xue, H. Gao, W. D. Nix, and Z. C. Xia, "A study of microindentation hardness tests by mechanism-based strain gradient plasticity," *Journal of Materials Research*, vol. 15, no. 8, pp. 1786–1796, 2000.

[49] S. Nikolov, C.-S. Han, and D. Raabe, "On the origin of size effects in small-strain elasticity of solid polymers," *International Journal of Solids and Structures*, vol. 44, no. 5, pp. 1582–1592, 2007.

[50] C.-S. Han and S. Nikolov, "Indentation size effects in polymers and related rotation gradients," *Journal of Materials Research*, vol. 22, no. 6, pp. 1662–1672, 2007.

[51] S. Swaddiwudhipong, L. H. Poh, J. Hua, Z. S. Liu, and K. K. Tho, "Modeling nano-indentation tests of glassy polymers using finite elements with strain gradient plasticity," *Materials Science and Engineering A*, vol. 404, no. 1-2, pp. 179–187, 2005.

[52] T.-Y. Zhang, W.-H. Xu, and M.-H. Zhao, "The role of plastic deformation of rough surfaces in the size-dependent hardness," *Acta Materialia*, vol. 52, no. 1, pp. 57–68, 2004.

[53] W. C. Oliver and G. M. Pharr, "Improved technique for determining hardness and elastic modulus using load and displacement sensing indentation experiments," *Journal of Materials Research*, vol. 7, no. 6, pp. 1564–1583, 1992.

[54] ISO, "Metallic materials—instrumented indentation test for hardness and materials parameters: Part 1: test method," Tech. Rep. 14577-1, International Organization for Standardization, 2002.

[55] A. C. Fischer-Cripps, *Nanoindentation*, Springer, New York, NY, USA, 3rd edition, 2011.

[56] R. Saha and W. D. Nix, "Effects of the substrate on the determination of thin film mechanical properties by nanoindentation," *Acta Materialia*, vol. 50, no. 1, pp. 23–38, 2002.

[57] R. Rodríguez and I. Gutierrez, "Correlation between nanoindentation and tensile properties influence of the indentation size effect," *Materials Science and Engineering A*, vol. 361, no. 1-2, pp. 377–384, 2003.

[58] J. A. Tjernlund, E. K. Gamstedt, and Z.-H. Xu, "Influence of molecular weight on strain-gradient yielding in polystyrene," *Polymer Engineering & Science*, vol. 44, no. 10, pp. 1987–1997, 2004.

[59] C.-S. Han, S. H. R. Sanei, and F. Alisafaei, "On the origin of indentation size effect and depth dependent mechanical properties of elastic polymers," *Journal of Polymer Engineering*, 2015.

[60] J. K. Deuschle, G. Buerki, H. M. Deuschle, S. Enders, J. Michler, and E. Arzt, "In situ indentation testing of elastomers," *Acta Materialia*, vol. 56, no. 16, pp. 4390–4401, 2008.

[61] A. Flores and F. J. Baltá Calleja, "Mechanical properties of poly(ethylene terephthalate) at the near surface from depth-sensing experiments," *Philosophical Magazine A*, vol. 78, no. 6, pp. 1283–1297, 1998.

[62] C. A. Tweedie, G. Constantinides, K. E. Lehman, D. J. Brill, G. S. Blackman, and K. J. Van Vliet, "Enhanced stiffness of amorphous polymer surfaces under confinement of localized contact loads," *Advanced Materials*, vol. 19, no. 18, pp. 2540–2546, 2007.

[63] Y. Hu, L. Shen, H. Yang et al., "Nanoindentation studies on Nylon 11/clay nanocomposites," *Polymer Testing*, vol. 25, no. 4, pp. 492–497, 2006.

[64] R. V. S. Tatiraju, C.-S. Han, and S. Nikolov, "Size dependent hardness of polyamide/imide," *The Open Mechanics Journal*, vol. 2, no. 1, pp. 89–92, 2008.

[65] W. W. Gerberich, N. I. Tymiak, J. C. Grunlan, M. F. Horstemeyer, and M. I. Baskes, "Interpretations of indentation size effects," *ASME Journal of Applied Mechanics*, vol. 69, no. 4, pp. 433–442, 2002.

[66] N. I. Tymiak, D. E. Kramer, D. F. Bahr, T. J. Wyrobek, and W. W. Gerberich, "Plastic strain and strain gradients at very small indentation depths," *Acta Materialia*, vol. 49, no. 6, pp. 1021–1034, 2001.

[67] C.-S. Han, "Indentation size effect in polymers," in *Advances in Materials Science Research*, M. C. Wythers, Ed., vol. 10, chapter 15, pp. 393–413, Nova Science, New York, NY, USA, 2011.

[68] C.-S. Han, "Influence of the molecular structure on indentation size effect in polymers," *Materials Science and Engineering A*, vol. 527, no. 3, pp. 619–624, 2010.

[69] X. Li and B. Bhushan, "Continuous stiffness measurement and creep behavior of composite magnetic tapes," *Thin Solid Films*, vol. 377-378, pp. 401–406, 2000.

[70] T. K. Chaki and J. C. M. Li, "Latent hardening in high–density polyethylene," *Journal of Applied Physics*, vol. 56, no. 9, pp. 2392–2395, 1984.

[71] L. Shen, I. Y. Phang, L. Chen, T. Liu, and K. Zeng, "Nanoindentation and morphological studies on nylon 66 nanocomposites. I. Effect of clay loading," *Polymer*, vol. 45, no. 10, pp. 3341–3349, 2004.

[72] L. Shen, I. Y. Phang, T. Liu, and K. Zeng, "Nanoindentation and morphological studies on nylon 66/organoclay nanocomposites. II. Effect of strain rate," *Polymer*, vol. 45, no. 24, pp. 8221–8229, 2004.

[73] T. Liu, I. Y. Phang, L. Shen, S. Y. Chow, and W.-D. Zhang, "Morphology and mechanical properties of multiwalled carbon nanotubes reinforced nylon-6 composites," *Macromolecules*, vol. 37, no. 19, pp. 7214–7222, 2004.

[74] L. Shen, I. Y. Phang, and T. Liu, "Nanoindentation studies on polymorphism of nylon 6," *Polymer Testing*, vol. 25, no. 2, pp. 249–253, 2006.

[75] W. D. Zhang, L. Shen, I. Y. Phang, and T. Liu, "Carbon nanotubes reinforced nylon-6 composite prepared by simple melt-compounding," *Macromolecules*, vol. 37, no. 2, pp. 256–259, 2004.

[76] G. Chandrashekar, F. Alisafaei, and C.-S. Han, "Length scale dependent deformation in natural rubber," *Journal of Applied Polymer Science*, 2015.

[77] J. K. Deuschle, H. M. Deuschle, S. Enders, and E. Arzt, "Contact area determination in indentation testing of elastomers," *Journal of Materials Research*, vol. 24, no. 3, pp. 736–748, 2009.

[78] J. Deuschle, S. Enders, and E. Arzt, "Surface detection in nanoindentation of soft polymers," *Journal of Materials Research*, vol. 22, no. 11, pp. 3107–3119, 2007.

[79] J. K. Deuschle, E. J. de Souza, E. Arzt, and S. Enders, "Nanoindentation studies on cross linking and curing effects of PDMS,"

International Journal of Materials Research, vol. 101, no. 8, pp. 1014–1023, 2010.

[80] K. L. Johnson, *Contact Mechanics*, Cambridge University Press, 1985.

[81] I. N. Sneddon, "The relation between load and penetration in the axisymmetric boussinesq problem for a punch of arbitrary profile," *International Journal of Engineering Science*, vol. 3, no. 1, pp. 47–57, 1965.

[82] L. E. Govaert, P. H. M. Timmermans, and W. A. M. Brekelmans, "The influence of intrinsic strain softening on strain localization in polycarbonate: modeling and experimental validation," *Journal of Engineering Materials and Technology, Transactions of the ASME*, vol. 122, no. 2, pp. 177–185, 2000.

[83] F. Yang, A. C. M. Chong, D. C. C. Lam, and P. Tong, "Couple stress based strain gradient theory for elasticity," *International Journal of Solids and Structures*, vol. 39, no. 10, pp. 2731–2743, 2002.

[84] G. Kaupp, *Atomic Force Microscopy, Scanning Nearfield Optical Microscopy and Nanoscratching*, Application to Rough and Natural Surfaces, Springer, 2006.

[85] N. Garg and C.-S. Han, "A penalty finite element approach for couple stress elasticity," *Computational Mechanics*, vol. 52, no. 3, pp. 709–720, 2013.

[86] N. Garg and C.-S. Han, "Axisymmetric couple stress elasticity and its finite element formulation with penalty terms," *Archive of Applied Mechanics*, vol. 85, no. 5, pp. 587–600, 2015.

[87] N. Garg, F. Alisafaei, G. Chandrashekar, and C.-S. Han, "Fiber diameter dependent deformation in polymer composites—a numerical study," Submitted.

[88] L. Shen, W. C. Tjiu, and T. Liu, "Nanoindentation and morphological studies on injection-molded nylon-6 nanocomposites," *Polymer*, vol. 46, no. 25, pp. 11969–11977, 2005.

[89] D. M. Ebenstein, "Nano-JKR force curve method overcomes challenges of surface detection and adhesion for nanoindentation of a compliant polymer in air and water," *Journal of Materials Research*, vol. 26, no. 8, pp. 1026–1035, 2011.

[90] F. Carrillo, S. Gupta, M. Balooch et al., "Nanoindentation of polydimethylsiloxane elastomers: effect of crosslinking, work of adhesion, and fluid environment on elastic modulus," *Journal of Materials Research*, vol. 20, no. 10, pp. 2820–2830, 2005.

[91] Y. Cao, D. Yang, and W. Soboyejoy, "Nanoindentation method for determining the initial contact and adhesion characteristics of soft polydimethylsiloxane," *Journal of Materials Research*, vol. 20, no. 8, pp. 2004–2011, 2005.

[92] D. M. Ebenstein and K. J. Wahl, "A comparison of JKR-based methods to analyze quasi-static and dynamic indentation force curves," *Journal of Colloid and Interface Science*, vol. 298, no. 2, pp. 652–662, 2006.

[93] S. Gupta, F. Carrillo, C. Li, L. Pruitt, and C. Puttlitz, "Adhesive forces significantly affect elastic modulus determination of soft polymeric materials in nanoindentation," *Materials Letters*, vol. 61, no. 2, pp. 448–451, 2007.

[94] J. D. Kaufman and C. M. Klapperich, "Surface detection errors cause overestimation of the modulus in nanoindentation on soft materials," *Journal of the Mechanical Behavior of Biomedical Materials*, vol. 2, no. 4, pp. 312–317, 2009.